https://doi.org/10.5194/egusphere-2025-294
Preprint. Discussion started: 24 February 2025

Effects of different emission inventories on tropospheric ozone and methane lifetime

Catherine Acquah[1], Laura Stecher[1], Mariano Mertens[1,2], and Patrick Jöckel[1]

[1]Deutsches Zentrum für Luft- und Raumfahrt, Institut für Physik der Atmosphäre, Oberpfaffenhofen, Germany
[2]Faculty of Aerospace Engineering, Section Operations and Environment, Delft University of Technology, 2629 HS, Delft, The Netherlands

Correspondence: Patrick Jöckel (Patrick.Joeckel@dlr.de)

Abstract. This study assesses the influence of anthropogenic emission inventories of ozone (O_3) precursor species (i.e., NO_x, CO and NMHCs) prescribed in the simulations of the two phases of the Chemistry-Climate Model Initiative (CCMI) on tropospheric O_3, the hydroxyl radical (OH) and the methane (CH_4) lifetime. We performed two transient simulations for the period 2000 - 2010 with the chemistry-climate model EMAC, one prescribing the emission inventory of CCMI-1, and the other that of CCMI-2022. Using the tagging approach, we attribute the differences of O_3, OH and the tropospheric CH_4 lifetime to individual emission sectors. It is, to our knowledge, the first application of the tagging approach to attribute changes of the simulated CH_4 lifetime to individual emission sectors.

The emission inventory used for CCMI-2022 leads to a 3.7% larger tropospheric O_3 column, and to a 3.2% shorter tropospheric CH_4 lifetime compared to CCMI-1 in the northern hemisphere. In the southern hemisphere, the tropospheric O_3 column is 4.5% larger, and the tropospheric CH_4 lifetime 4.3% shorter. Differences in tropospheric O_3 are largely driven by changes of emissions from the anthropogenic non-traffic and land transport sectors in the northern hemisphere. In the southern hemisphere, the primary contributors are emissions from anthropogenic non-traffic, biomass burning and shipping. These sectors also play a significant role in reducing the simulated tropospheric CH_4 lifetime. However, the contribution of a particular sector to changes in O_3 does not necessarily align with its impact on the CH_4 lifetime.

1 Introduction

Tropospheric ozone (O_3), a greenhouse gas, plays a significant role in influencing both, climate and air quality (Haagensmit, 1952; Stevenson et al., 2013). It adversely affects human health and vegetation. Anthropogenic activities, including industry and land transport, release O_3 precursors such as nitrogen oxides (NO_x), non-methane hydrocarbons (NMHCs), and carbon monoxide (CO), affecting air quality. Model data indicate an increase of about 30% of the total mass of tropospheric O_3 between 1850 and 2010 (Lamarque et al., 2005; Young et al., 2013). As a greenhouse gas in the middle and upper troposphere, O_3 contributes to positive radiative forcing and consequently to global warming (Stevenson et al., 2013). Next to its role as a

https://doi.org/10.5194/egusphere-2025-294
Preprint. Discussion started: 24 February 2025

greenhouse gas, tropospheric O_3 is one key component of photochemical smog (Haagensmit, 1952). As an air pollutant, during prolonged periods of fair-weather conditions, high ground level O_3 concentrations can have adverse effects on human health (Nuvolone et al., 2018). Some studies have already demonstrated an increased mortality after prolonged exposure (Bell et al., 2004; Jerrett et al., 2009; Silva et al., 2013). Concentrations of tropospheric O_3 and its precursors are significantly elevated in many regions, not only due to road traffic (Niemeier et al., 2006), but also due to industrial processes, biomass burning (Seinfeld and Pandis, 2016) as well as biogenic emissions (Seinfeld and Pandis, 2016). Another relevant aspect relates to the phytotoxicity of tropospheric O_3, as it is one of the most potent air pollutants for plants (Ashmore, 2005; Wedow et al., 2021). Various studies have demonstrated the reduction of agricultural crop yields (Emberson et al., 2018; Iglesias et al., 2006) and damage to broadleaves (Moura et al., 2014). The photochemical production of O_3 in the troposphere is non-linearly dependent on various precursors, such as NO_x, CO, and NMHCs (Bourtsoukidis et al., 2019; Crutzen, 1974). NO_x emissions from anthropogenic sources originate e.g. from industry, land transport, aviation, and shipping (e.g., Uherek et al., 2010). Natural NO_x is emitted from soil and produced by lightning discharges (e.g., Schumann and Huntrieser, 2007; Vinken et al., 2014). According to Seinfeld and Pandis (2016), two-thirds of CO is emitted from anthropogenic activities, including the oxidation of anthropogenically produced methane (CH_4). The origin of natural NMHC emissions are marine and terrestrial environments, e.g., vegetation (Guenther et al., 1995).

An important aspect of tropospheric O_3 is its role as a source of the hydroxyl radical (OH), which is a very relevant oxidant in the atmosphere (Monks, 2005), and thus largely determines the self-cleansing capacity of the troposphere (Monks et al., 2015). The abundance of OH influences the atmospheric lifetime of the greenhouse gas CH_4, as the oxidation with OH represents the most important sink of atmospheric CH_4 (Lelieveld et al., 2016; Voulgarakis et al., 2013; Saunois et al., 2020). CH_4 decomposition by OH is considered as a source of NMHCs (Seinfeld and Pandis, 2016), which in turn are part of tropospheric O_3 production process (Crutzen, 1974), and thus the OH formation links the processes of CH_4 decomposition and tropospheric O_3 production and vice versa. According to the IPCC Sixth Assessment Report (IPCC, 2021) CH_4 is the second-most important greenhouse gas directly emitted by human activity. Different studies demonstrate the wide range of uncertainty of CH_4 lifetime estimates, which is the reason why the investigation of the CH_4 lifetime remains an important research topic. In particular, neither OH (on the global scale), nor the CH_4 lifetime, can be observed directly. Therefore, estimates of the CH_4 lifetime are derived from observations of species with known emissions, whose main sink is the oxidation with OH, such as methylchloroform (CH_3CCl_3) (Krol et al., 1998; Prinn et al., 2005; Montzka et al., 2011) or ^{14}CO (Brenninkmeijer et al., 1992; Jöckel et al., 2002; Manning et al., 2005). Estimates of the CH_4 lifetime based on observations of CH_3CCl_3 are, for example, 10.2 (+0.9 -0.7) years (Prinn et al., 2005) and 9.1 $\pm$ 0.9 years (Prather et al., 2012). The CMIP6 AerChemMIP model ensemble as analyzed by Stevenson et al. (2020) suggests a whole-atmosphere CH_4 lifetime of 8.4 $\pm$ 0.3 years for the present-day, while the two most recent IPCC Reports state a lifetime of 9.25 $\pm$ 0.6 years (Myhre et al., 2013) and 9.1 $\pm$ 0.9 years (Szopa et al., 2021), respectively. Anthropogenic emissions of NO_x and CO impacting the OH abundance have influenced the development of atmospheric CH_4 concentrations in recent decades (Stevenson et al., 2020; Skeie et al., 2023).

To summarize, O_3 precursors strongly influence tropospheric O_3 and CH_4 lifetime. The determination of O_3 precursor emissions is not trivial, and emission inventories are subject to large uncertainties. Hoesly et al. (2018) suggest, that the

https://doi.org/10.5194/egusphere-2025-294
Preprint. Discussion started: 24 February 2025

uncertainties can range from ±8% - ±176%. The tropospheric O_3, OH and CH_4 lifetime simulated by chemistry-climate models (CCMs) largely depends on the choice of the emission inventory. The two phases of the Chemistry-Climate Model Initiative (CCMI) use different emission inventories (see CCMI-1 simulation protocol; CCMI-2 simulation protocol). CCMI-1 uses the MACCity emissions inventory (Granier et al., 2011), whereas CCMI-2022 uses the Community Emissions Data System (CEDS; Hoesly et al., 2018), which has been also used by AerChemMIP, which is endorsed in the Coupled Model Intercomparison Project 6 (CMIP6) (Collins et al., 2017). The latter multi-model comparison initiatives form an important groundwork for the IPCC reports (IPCC, 2013, 2021). Comparing the EMAC (ECHAM5/ MESSy Atmospheric Chemistry) simulations performed for the two different phases of CCMI, it was noticed that the resulting CH_4 lifetime was considerably shorter in the simulations performed for the second phase of CCMI (see Fig. 1). One reason for the shorter lifetime is the changed emission inventory of O_3 precursor species.

In this study, we therefore specifically examine the effect of the modified emission inventories on the tropospheric O_3 abundance and the CH_4 lifetime. For this purpose, we performed targeted simulations with the EMAC model, prescribing either the emission inventory of CCMI-1 or CCMI-2022 for O_3 precursor species. The tropospheric CH_4 lifetime corresponding to these simulations are shown by the red curves in Fig. 1. The changed prescribed emission inventories can not explain the full difference of tropospheric CH_4 lifetime between the EMAC simulations originally performed for CCMI-1 and CCMI-2022 (blue and black curves in Fig. 1). There have been further model developments and setup changes from CCMI-1 to CCMI-2022 that have, however, all been used for the tageted simulations performed for this study (red curves) and that we address in the supplement.

Further, we use the tagging approach to attribute the O_3 and CH_4 lifetime differences caused by the changed prescribed emissions to individual emission sectors. Some previous studies have successfully applied the tagging approach for determining the contributions of specific source categories to the tropospheric O_3 (Butler et al., 2020; Grewe et al., 2012, 2010, 2017; Mertens et al., 2018, 2020; Rieger et al., 2018; Kilian et al., 2024), while the tagging method to attribute CH_4 lifetime differences has, to our knowledge, been applied only once (Mertens et al., 2024).

The paper is structured as follows: Section 2 describes the used CCM EMAC shortly and explains the simulation set-up including information about the used emission inventories, the tagging method and the method to calculate the tropospheric CH_4 lifetime. Section 3 shows the results, i.e. the impact of the modified emission inventory on tropospheric O_3, OH and the CH_4 lifetime. It is followed by a discussion in Sect. 4 including limitations of the applied tagging method and the simulation set-up, as well as a comparison to other studies. We close with a summary of our findings and some concluding remarks in Sect. 5.

2 Methods and Data

To determine the impact of the two emission inventories on tropospheric O_3 and CH_4 lifetime, we perform targeted simulations with the EMAC model in which either one or the other inventory is prescribed. In the following sections, the EMAC model, the simulation set-up including information about the emission inventories, and the tagging method as well as the calculation

https://doi.org/10.5194/egusphere-2025-294
Preprint. Discussion started: 24 February 2025

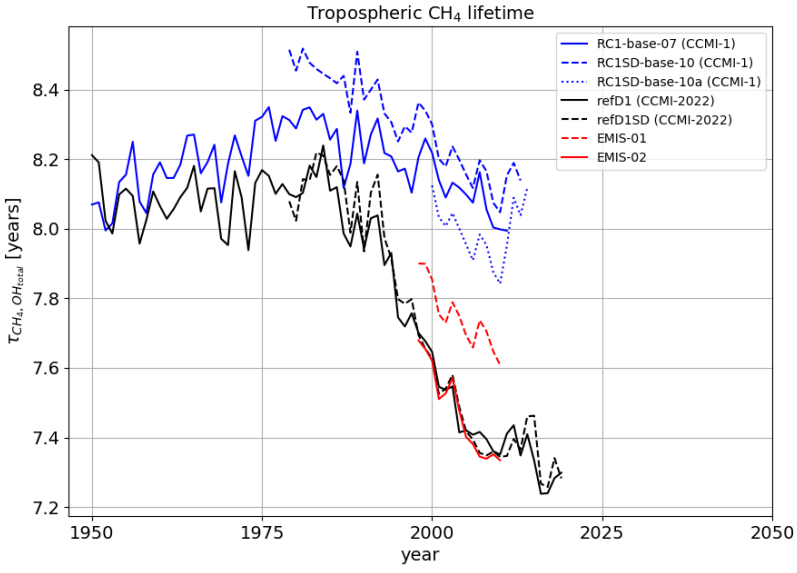

Figure 1. Tropospheric CH_4 lifetime with respect to the oxidation with OH, $\tau_{CH_4,OH_{total}}$, for the EMAC simulations performed for phase 1 of CCMI (CCMI-1) in blue, phase 2 of CCMI (CCMI-2022) in black, and of the simulations analyzed in the present study, EMIS-01 and EMIS-02, in red. See Jöckel et al. (2016) for details of the setup of the CCMI-1 simulations and Jöckel (2023) for refd1.

of the CH_4 lifetime are described. In Sect. 2.3 we also describe the two methods to estimate the contribution of the various categories to the overall change of the CH_4 lifetime.

2.1 Model description

We perform simulations with the global chemistry-climate model EMAC (ECHAM/MESSy Atmospheric Chemistry). The EMAC model is composed of the European Center Hamburg Model version 5 (ECHAM5; Roeckner et al., 2006) as the dynamical base model and the Modular Earth Submodel System (MESSy; Jöckel et al., 2010). MESSy describes meteorological processes and atmospheric chemistry in a modular framework (Jöckel et al., 2010). The MESSy approach flexibly combines individual submodels with a base model (Jöckel et al., 2005). These submodels describe processes in the troposphere and middle atmosphere and their interaction with oceans, land, and anthropogenic influences (Jöckel et al., 2010).

https://doi.org/10.5194/egusphere-2025-294
Preprint. Discussion started: 24 February 2025

Simulation name	ozone precursor emissions	GHG lower boundary condition (incl. methane)	ODS
EMIS-01	CCMI-1	CCMI-1	CCMI-1
EMIS-01-ODS	CCMI-1	CCMI-1	CCMI-2022
EMIS-02	CCMI-2022	CCMI-2022	CCMI-2022

Table 1. Overview of the performed numerical experiments.

2.2 Simulation strategy

2.2.1 Set-up information

EMAC was applied in T42L90MA resolution, i.e. at a triangular (T) truncation at wave number 42 of the spectral dynamical core, corresponding to a quadratic Gaussian grid of approximately $2.8^\circ \times 2.8^\circ$ resolution in latitude and longitude and 90 vertical levels, with the uppermost level centered around 0.01 hPa (≈ 80 km height) in the middle atmosphere (MA).

Overall, we performed three different simulations as listed in Table 1. The simulations EMIS-01 and EMIS-02 differ between the used emission inventories for shorter lived chemical species (i.e. NO_x, CO, SO_2, NH_3, and VOCs, see Sect. 2.2.2 for more details), the prescribed surface mixing ratios of GHGs (in particular also CH_4), and the prescribed ozone depleting substances (ODS) surface mixing ratios (see Jöckel et al., 2016, for more details). The global mean surface CH_4 mixing ratio is about 0.01 ppm larger in the simulation EMIS-02 compared to EMIS-01 (see Fig. S10 in the supplement), which is expected to cause a small extension of the CH_4 lifetime, which counteracts the overall shortening of the CH_4 lifetime. The lower boundary for N_2O is nearly identical, which is also reflected by the total mass of N_2O (see Fig. S11 in the supplement). The influence of the changed prescribed ODS turned out to have no influence on the CH_4 lifetime and only a small influence on tropospheric O_3 (see Fig. S2 in the supplement). Therefore, only the simulations EMIS-01 and EMIS-02 are further analysed in our study.

To decouple dynamics from chemistry, EMAC was operated in quasi chemistry-transport model (QCTM) mode (Deckert et al., 2011). In this mode, mixing ratios of radiatively active constituents are prescribed for the radiation calculations, and the hydrological cycle is decoupled from the chemistry. This assures that differences of the emission inventories prescribed in the two simulations do not affect the model's meteorology. Accordingly, differences of the chemical decomposition between the results of EMIS-01 and EMIS-02 occur solely due to differences in the emissions and prescribed surface mixing ratios of CH_4 and GHGs.

For the calculation of lighting NO_x emissions we use the parameterization by Grewe et al. (2001). Biogenic C_5H_8 emissions and soil NO_x emissions are calculated with the submodel ONEMIS (Kerkweg et al., 2006) applying the parameterization of Guenther et al. (1995) and Yienger and Levy II (1995), respectively. Due to the binary identical meteorology between the simulations, these online calculated, meteorology dependent emissions are also binary identical in both simulations.

Nudging by Newtonian relaxation towards ECMWF ERA-5 reanalysis data (Hersbach et al., 2020) was performed aiming at a realistic representation of the meteorological situation at a given time. Nudged are the temperature, divergence, vorticity, and the logarithm of surface pressure (Jöckel et al., 2016). Wave zero of the temperature (e.g. the mean temperature) is not nudged.

https://doi.org/10.5194/egusphere-2025-294
Preprint. Discussion started: 24 February 2025

We investigated the period 2000 – 2010, with a spin-up phase for the simulations comprising 1998 and 1999. The model output is originally output in netCDF format with global data coverage as snapshots every 10 h of simulated time on model levels. Based on this, monthly averages are calculated on pressure levels.

2.2.2 Emission inventories

The emission inventory for CCMI-1 is based on the MACCity emission inventory (Granier et al., 2011), an extension of the Atmospheric Chemistry and Climate Model Intercomparison Project (ACCMIP) emissions dataset based on 1960 and 2000, as well as 2005 and 2010 RCP 8.5 emissions (CCMI-1 simulation protocol). The emission inventory for CCMI-1 contains anthropogenic emissions based on the product of estimates for activity data from country records and international organizations and emission factors (Granier et al., 2011). The basis for global biomass burning emissions are satellite data (Granier et al., 2011). The MACCity inventory includes global emissions of CO, NO_x and NMHCs, whereby it considers a monthly resolved seasonal cycle (Granier et al., 2011). The ACCMIP dataset according to Lamarque et al. (2005) was expanded and calculated for emissions from biomass burning on the basis of the annual monthly average trace gas emissions from the spatially and temporally modified RETRO (REanalysis of the TROpospheric chemical composition; Schultz et al., 2007) carbon emissions data from GFED-v2 (Global Fire Emissions Database; van der Werf et al., 2006) for 1997 to 2008 (Granier et al., 2011). A detailed description of the implementation of the emission inventory for EMAC is provided in the supplement of Jöckel et al. (2016).

The basis of the emission inventory for CCMI-2022 is the Community Emissions Data System (CEDS) dataset, which includes annual historical (1750 – 2014) anthropogenic emissions for the species CO, NO_x, and NMHCs (Hoesly et al., 2018). The dataset includes existing energy consumption data, and regional and country emission inventories. The dataset provides annual emissions at country and sector level with monthly seasonal variations. The biomass burning emissions in CCMI-2022 are according to van Marle et al. (2017).

Time series of the years 2000 - 2010 of global emissions of NO_x, NMHCs and CO for individual sectors anthropogenic non-traffic, biogenic, land transport, shipping, biomass burning and aviation, as prescribed in the simulations EMIS-01 or EMIS-02 can be found in the supplement (Figures S6, S7 and S8). Global anthropogenic NO_x emissions are larger by 8.70 Tg(N) $year^{-1}$ on average for the period 2000 - 1010 for the simulation EMIS-02 compared to EMIS-01 (see Tab. 3). In the NH, the sectors anthropogenic non-traffic, land transport and shipping contribute most to the difference in total NO_x emissions, with NO_x emissions being larger in the EMIS-02 simulation than in EMIS-01. In the SH, the largest contributors to the NO_x emission difference are the sectors biomass burning and shipping (see Tab. 3). The difference of NO_x emissions from shipping between EMIS-01 and EMIS-02 peaks in the year 2008 (see Fig. S6 in the supplement), as the emission prescribed for EMIS-02 account for the increase of shipping emissions until 2008 and the decline after 2008 (Hoesly et al., 2018).

Global CO emissions are reduced by 30.14 Tg(C) $year^{-1}$ on average for the period 2000 - 2010 for EMIS-02 compared to EMIS-01 (see Tab. 3). The reduction is dominated by the biomass burning sector in both hemispheres, whereas CO emissions from the anthropogenic non-traffic and land transport sectors are larger in EMIS-02 (see Tab. 3).

https://doi.org/10.5194/egusphere-2025-294
Preprint. Discussion started: 24 February 2025

Global NMHC emissions are enhanced by 56.89 Tg(C) year^{-1} on average for the period 2000 - 2010 for EMIS-02 (see Tab. 3). The increase is dominated by the anthropogenic non-traffic sector, followed by biomass burning and land transport in the NH. In the SH, differences in the anthropogenic non-traffic and biomass burning sectors contribute most as well.

2.2.3 TAGGING for source attribution

To understand the effects of the emission changes on O_3 precursors, O_3 and OH in more detail, we apply the TAGGING submodel as described by Grewe et al. (2017); Rieger et al. (2018). The TAGGING submodel as technical implementation of the tagging approach, a labeling technique, is used to diagnose contributions of individual source categories to the mixing ratio of tropospheric O_3 (Grewe et al., 2010). For this purpose, the TAGGING submodel distributes the calculated chemical production rates among the different tagged categories (Grewe et al., 2012). Tracer mixing ratios and chemical production by specific chemical reactions are provided by the submodel Module Efficiently Calculating the Chemistry of the Atmosphere (MECCA; Sander et al., 2019) (Grewe et al., 2017). According to Grewe et al. (2017), tagged species are NO_y, NMHCs, CO, PAN, O_3, HO_2, and OH. For these chemical species additional tracers for each source category reflect the contribution of the respective category to the resulting mixing ratio of the corresponding species. In this study, we use the TAGGING submodel v1.1 according to Rieger et al. (2018), which was updated to be consistent with the used chemical mechanism. Thereby, the changed partitioning of the O_3 production rates is the most important adjustment, whereas the TAGGING for OH and HO_2 remained unchanged (see Stecher, 2024, Chapter 3.1.6 for more details). TAGGING follows a steady-state approach to calculate the contributions of the emissions to the mixing ratios of OH/HO_2 according to Rieger et al. (2018). Since the rate of O_3 production depends on precursor concentrations, the O_3 production rate must be distributed among the categories by a combinatorial redistribution according to the concentrations of the tagged species (Grewe et al., 2017). According to Grewe et al. (2017), "all possible combinations between a tagged NO_x species and another tagged HO_x species are evaluated and their probability calculated in accordance with the chemical production rate calculation".

In this study, we investigate ten source categories (also referred to as tagging categories in the further course of this text) and their contribution to tropospheric O_3, OH, and the CH_4 lifetime. The latter is derived from the tagged OH as explained in Sect. 2.3 in more detail. We use the same definition of tagging categories as Grewe et al. (2017), distinguishing between natural and anthropogenic sources. The definition of the ten tagging categories is listed in Table 2.

2.3 Calculation of methane lifetime

In this study, we calculate the (tropospheric) CH_4 lifetime with respect to the oxidation with OH according to Jöckel et al. (2016) as

$$\tau_{CH_4,OH_{total}} = \frac{\sum\limits_{b\in B} m_{CH_4}}{\sum\limits_{b\in B} k_{CH_4+OH}(T)\cdot c_{air}(T,p,q)\cdot OH\cdot m_{CH_4}}, \quad (1)$$

with m_{CH_4} being the mass of CH_4 in [kg], $k_{CH_4+OH}(T)$ the temperature T dependent reaction rate coefficient of the reaction $CH_4 + OH \rightarrow$ products in [cm^3 s^{-1}], c_{air} the concentration of air in [cm^{-3}] and OH the mole fraction of OH in [mol mol^{-1}]

https://doi.org/10.5194/egusphere-2025-294
Preprint. Discussion started: 24 February 2025

Table 2. Overview of the categories for the tagging source attribution applied in this study. Detailed definitions of the categories are given by Grewe et al. (2017). The anthropogenic non traffic category contains all non-traffic related activities i.e. industry, households, energy, and agriculture including agricultural waste burning

name	abbreviation	anthropogenic/natural	description
anthropogenic non-traffic	IND	anthropogenic	anthropogenic emissions not related to transport
land transport	TRA	anthropogenic	land transport (IPCC codes 1A3b_c_e) emissions
shipping	SHP	anthropogenic	Global shipping emissions (IPCC code 1A3d)
aviation	AIR	anthropogenic	Global aviation emissions
stratosphere	STR		downward transport from the stratosphere (more specifically, production of ozone by O_2)
biogenic	SOIL	natural	biogenic emissions and soil-NO_x
biomass burning	BIO	anthropogenic	emissions from biomass burning
CH4	CH4	both	degradation of CH_4 as source of NMHCs
N2O	N2O	both	degradation of N_2O as source of NO_y
lightning	LIG	natural	emissions of lightning NO_x

in all grid boxes b ∈ B. B is the region, for which the lifetime should be calculated, e.g. all grid boxes below the tropopause for the mean tropospheric lifetime, and all grid boxes below the tropopause in each hemisphere to derive a hemispheric CH_4 lifetime (denoted as SH and NH for the Southern and Northern Hemispheres, respectively). For the CH_4 lifetime calculation a climatological tropopause, defined as $tp_{clim} = 300\ \text{hPa} - 215\ \text{hPa} \cdot \cos^2(\phi)$, with ϕ being the latitude in degrees north, is used as recommended by Lawrence et al. (2001).

The CH_4 lifetime corresponding to the oxidation with OH of one tagging category is calculated by substituting the total OH in Eq. 1 by the TAGGING tracer OH_i, e.g. OH_{tra}.

$$\tau_{CH_4,OH_i} = \frac{\sum_{b\in B} m_{CH_4}}{\sum_{b\in B} k_{CH_4+OH}(T)\cdot c_{air}(T,p,q)\cdot OH_i \cdot m_{CH_4}}. \tag{2}$$

Note that for adding the CH_4 lifetimes of multiple categories the inverse of the sum of the reciprocals of individual CH_4 lifetimes needs to be calculated. For instance, the CH_4 lifetime of all categories is calculated as

$$\begin{aligned}\tau_{CH_4,sum} &= \Big(\sum_i \frac{1}{\tau_{CH_4,OH_i}}\Big)^{-1} \\ &= \Big(\frac{1}{\tau_{CH_4,OH_{ind}}} + \frac{1}{\tau_{CH_4,OH_{shp}}} + \frac{1}{\tau_{CH_4,OH_{bio}}} + \frac{1}{\tau_{CH_4,OH_{N2O}}} + \frac{1}{\tau_{CH_4,OH_{air}}} + \frac{1}{\tau_{CH_4,OH_{str}}} + ...\Big)^{-1}.\end{aligned} \tag{3}$$

Since not all source and loss reactions of OH, but a reduced reaction system, are considered by the TAGGING (Rieger et al., 2018), the sum of all OH TAGGING tracers can deviate from the total tracer OH. To quantify the deviation, we calculate the residuum lifetime, i.e. the CH_4 lifetime corresponding to CH_4 loss with the portion of OH that is unaccounted by the

https://doi.org/10.5194/egusphere-2025-294
Preprint. Discussion started: 24 February 2025

TAGGING as

$$\tau_{CH_4,res} = (\frac{1}{\tau_{CH_4,OH_{total}}} - \frac{1}{\tau_{CH_4,sum}})^{-1} = (\frac{1}{\tau_{CH_4,OH_{total}}} - \sum_i \frac{1}{\tau_{CH_4,OH_i}})^{-1}. \quad (4)$$

The difference between $\tau_{CH_4,OH_{total}}$ and $\tau_{CH_4,sum}$ excluding the residuum lifetime is about 0.1 years for both simulations. The mean values and the respective standard deviations (due to interannual variations) of $\tau_{CH_4,res}$ are 398.41 $\pm$ 40.99 years for EMIS-01 in the NH, 378.74 $\pm$ 89.30 years for EMIS-02 in the NH, 434.54 $\pm$ 49.52 years for EMIS-01 in the SH, and 339.56 $\pm$ 38.97 years for EMIS-02 in the SH, which is notably larger than the respective estimates of the other categories. Since the inverse of $\tau_{CH_4,res}$ determines the influence on the total CH_4 lifetime, we conclude that the CH_4 loss via oxidation with OH that is unaccounted by the TAGGING is sufficiently small. In particular, it is smaller than the contribution of any of the tagging categories. The total CH_4 lifetime $\tau_{CH_4,OH_{total}}$ and the sum over all tagging categories $\tau^*_{CH_4,sum}$ including $\tau_{CH_4,res}$ are identical, so that CH_4 loss by the total OH tracer is accounted for when $\tau_{CH_4,res}$ is included in Eq. 3.

In the results section, we attribute the change of the total CH_4 lifetime between the two simulations to the individual tagging categories. Therefore we calculate $\Delta\tau_{CH_4,i}$, which represents the lifetime reduction attributed to the emissions of category i. Note that $\Delta\tau_{CH_4,i}$ is not just given by the difference of CH_4 lifetimes of the category i between the two simulations, i.e. $\Delta\tau_{CH_4,i} \neq (\tau_{CH_4,OH_i}(\text{EMIS-02}) - \tau_{CH_4,OH_i}(\text{EMIS-01}))$, because of the fact that the reciprocals of individual CH_4 lifetimes need to be added when the sum of individual categories is calculated. We calculate $\Delta\tau_{CH_4,i}$ with two different methods, whose results are compared. For the first method, we derive a formula of the total lifetime $\tau_{CH_4,OH_{total}}$ (Eq. 1) in dependence of the lifetime of the category of interest τ_{CH_4,OH_i}, for which we calculate the derivative with respect to τ_{CH_4,OH_i}. Then, we approximate the derivative with the finite change of CH_4 lifetime, which results in the following relation for the lifetime reduction attributed to category i (see Appendix A for the derivation)

$$\Delta\tau_{CH_4,i} = \frac{(\tau_{CH_4,OH_{total}})^2}{(\tau_{CH_4,OH_i})^2} \cdot \Delta\tau_{CH_4,OH_i}. \quad (5)$$

For example, using this first method, $\Delta\tau_{CH_4,tra}$, which represents the contribution to the overall lifetime change attributed to the change of emissions (CCMI-2022 vs. CCMI-1) in a specific category, e.g. the category land transport, is calculated as

$$\Delta\tau^{M1}_{CH_4,tra} = \frac{\tau^2_{CH_4,OH_{total}}(\text{EMIS-01})}{\tau^2_{CH_4,tra}(\text{EMIS-01})} \cdot (\tau_{CH_4,OH_{tra}}(\text{EMIS-02}) - \tau_{CH_4,OH_{tra}}(\text{EMIS-01})). \quad (6)$$

For the second method, we exchange the CH_4 lifetime of the category of interest with the CH_4 lifetime of this category derived from the other simulation in Eq. 3. Thus, with the second method the contribution of the changed emissions of one category, e.g. land transport, to the overall lifetime change is calculated as

$$\Delta\tau^{M2}_{CH_4,tra} = (\frac{1}{\tau^*_{CH_4,sum}(\text{EMIS-01})} - \frac{1}{\tau^{exchanged}_{CH_4,OHtra}})^{-1}, \quad (7)$$

where $\tau^{exchanged}_{CH_4,tra}$ is calculated as

$$\tau^{exchanged}_{CH_4,OHtra} = (\frac{1}{\tau_{CH_4,OH_{tra}}(\text{EMIS-02})} + \sum_{i \neq tra} \frac{1}{\tau_{CH_4,OH_i}(\text{EMIS-01})})^{-1}. \quad (8)$$

https://doi.org/10.5194/egusphere-2025-294
Preprint. Discussion started: 24 February 2025

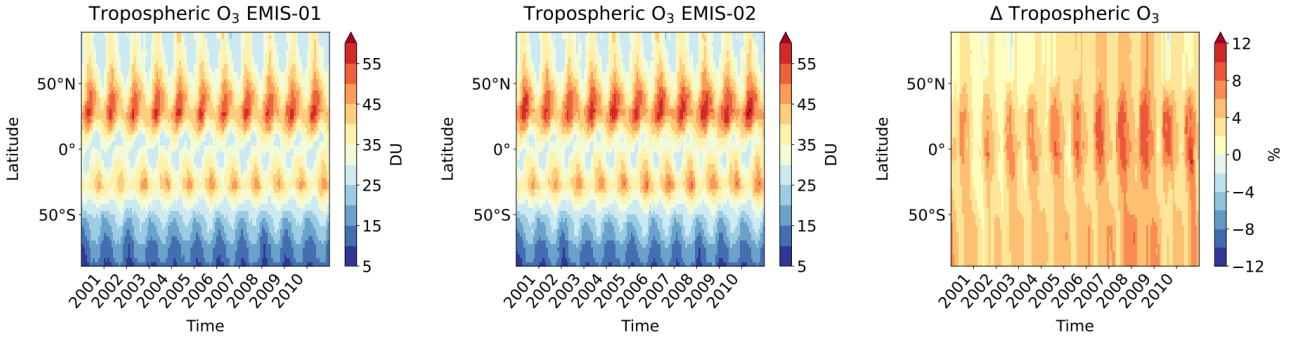

Figure 2. Tropospheric O_3 columns (DU) of the EMIS-01 and EMIS-02 simulation results and the relative differences with the EMIS-01 results as the reference. The data are monthly averaged for the period 2000 – 2010.

3 Results

3.1 Contribution to tropospheric ozone

In this section, we show the difference of total O_3 between the simulations EMIS-01 and EMIS-02, as well as the change of the contributions of individual tagging categories. The tropospheric O_3 columns (Fig. 2) in Dobson Units (DU) are presented as resulting from the EMIS-01 and EMIS-02 simulations as well as the relative differences in percent between both simulations for the period 2000 – 2010. The prognostic tropopause as diagnosed by the model is used as boundary between troposphere and stratosphere. The relative differences are calculated with the EMIS-01 results as the reference. The patterns of the tropospheric O_3 columns show the seasonal cycle of O_3, i.e. more O_3 is present in NH summer than in NH winter. In the NH, EMIS-02 ($\bar{x}$ = 38.88 DU; STD = 0.59) shows a 1.39 DU (= 3.7%) larger tropospheric O_3 column compared to EMIS-01 ($\bar{x}$ = 37.49 DU; STD = 0.05) for the period 2000 - 2010. In the SH, EMIS-02 ($\bar{x}$ = 27.90 DU; STD = 0.43) also shows larger values than EMIS-01 ($\bar{x}$ = 26.71 DU; STD = 0.32). The absolute difference averaged over the period 2000 - 2010 is 1.19 DU in the SH, which corresponds to 4.5%. The tropospheric O_3 column is especially high in the NH between 20° and 50°, showing values up to 60 DU. Within the period 2000 – 2010, the tropospheric O_3 column in the EMIS-02 simulation between 10°S and 40° N is up to 12% higher than in the EMIS-01 simulation. The maximum difference of the tropospheric O_3 column occurs in the years 2008 and 2009. Globally and temporally averaged, the simulation with the EMIS-02 emissions shows a 4% larger tropospheric O_3 column compared to EMIS-01.

The zonal mean of the total O_3 volume mixing ratio in nmol/mol and the differences between EMIS-01 and EMIS-02 are shown in Fig. S1 in the supplement. Figure 3 shows the relative zonal mean contribution of the categories shipping, anthropogenic non-traffic, land transport, aviation and biomass burning to total O_3, as well as the difference of the contribution between the two simulations. A corresponding plot for the categories N_2O decomposition, lightning, stratosphere, CH_4 and biogenic can be found in the supplement (Fig. S4). The differences between the O_3 contributions are a result of the complex

https://doi.org/10.5194/egusphere-2025-294
Preprint. Discussion started: 24 February 2025

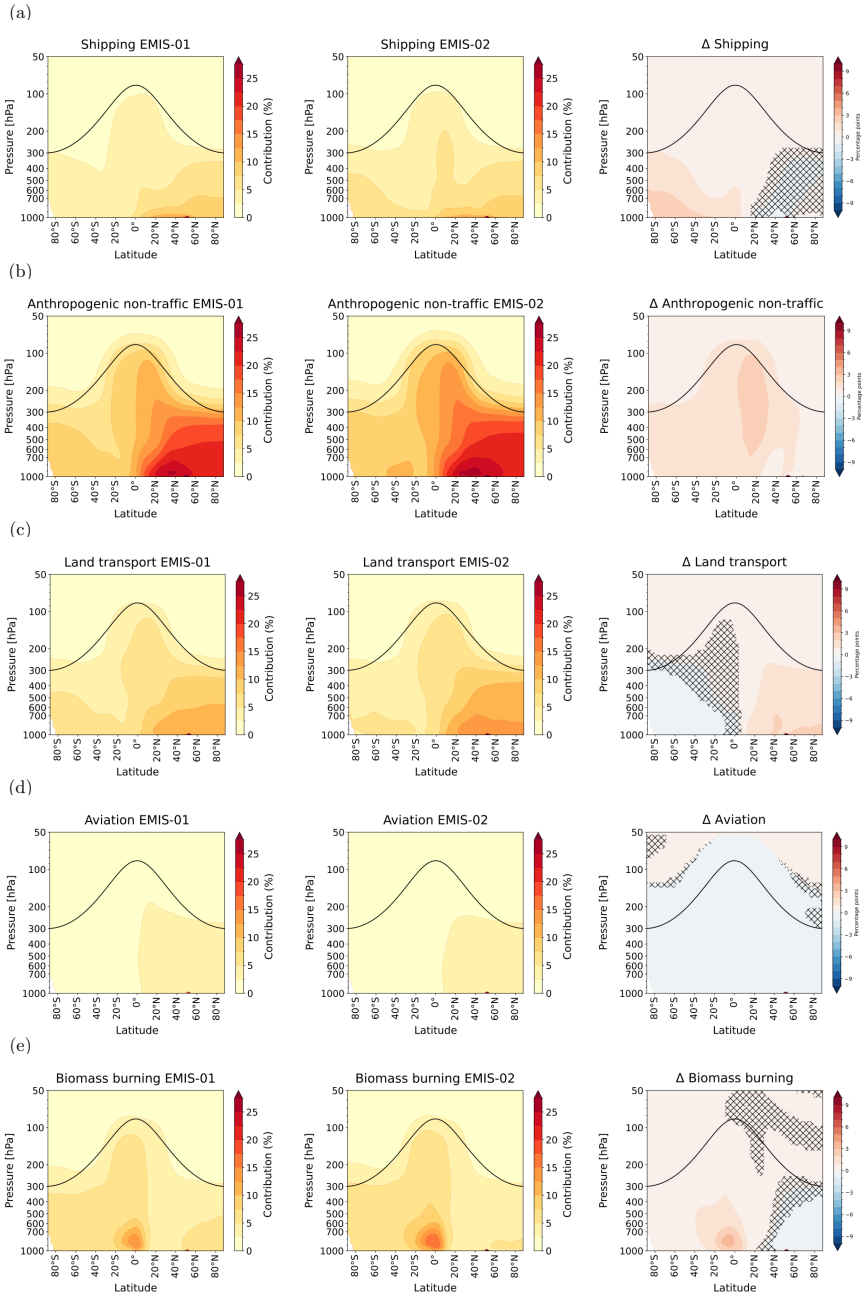

Figure 3. Relative contributions to total O_3 of the tagging categories (a) shipping, (b) anthropogenic non-traffic, (c) land transport (d) aviation and (e) biomass burning. The left and middle columns show the contribution of the respective category in the simulations EMIS-01 and EMIS-02, respectively. The right column shows the differences of the relative contributions to O_3 between the two simulation in percentage points. Zonal means of the years 2000 – 2010 are presented. Hatches in the delta plot indicate a p-value ≥ 0.05 from the dependent t-test for paired samples.

https://doi.org/10.5194/egusphere-2025-294
Preprint. Discussion started: 24 February 2025

interplay between the emission changes and the background chemistry. In the NH, especially land transport, anthropogenic non-traffic and shipping emissions are larger in EMIS-02 compared to EMIS-01 (see Sect. 2.2.2). However, only for land transport and anthropogenic emissions the contribution to O_3 are larger in EMIS-02 compared to EMIS-01 in the NH. For shipping emissions, the differences between EMIS-02 and EMIS-01 are not significant over most regions in the NH. The increase of the contributions from land transport and anthropogenic non-traffic emissions lead to a decrease of contributions from biomass burning in the NH in EMIS-02 compared to EMIS-01, even though the emissions are only slightly lower in EMIS-02 compared to EMIS-01. In the SH hemisphere, however, the strong increase of the biomass burning emissions in EMIS-02 lead to larger contributions in EMIS-02 compared to EMIS-01. The contribution of aviation emissions to O_3 is lower in EMIS-02 compared to EMIS-01, partly due to the slightly lower emissions, but also due to the artificially shifted aviation emissions from the tropics to the polar regions in the CEDS emission inventory as reported by Thor et al. (2023).

To understand the effects of the changed emissions onto O_3 production in more detail, we calculate the O_3 burden efficiency (see also Mertens et al., 2024), which is defined for example for the shipping category as:

$$\chi^{SHP} = \frac{\mathrm{B}(\mathrm{O_3^{SHP}})}{\mathrm{E}(\mathrm{NO_x^{SHP}})}. \tag{9}$$

In this definition, $\mathrm{B}(\mathrm{O_3^{SHP}})$ is the annual mean total atmospheric mass of O_3 attributed to shipping emissions (in kg), while $\mathrm{E}(\mathrm{NO_x^{SHP}})$ are the global annual mean shipping emissions of NO_x (in kg(N) per year).

Figure 4 shows the burden efficiency for the tagging categories, for which NO_x emissions are either prescribed or calculated online except for the category aviation. The aviation category is shown separately in Fig. S12 because it has a much larger burden efficiency (Mertens et al., 2024). The burden efficiency of the aviation category, χ^{AIR}, is larger in the simulation EMIS-02. The maximum difference of χ^{AIR} between the two simulations is about 10% in the year 2010 as χ^{AIR} of the simulation EMIS-01 decreases over the 11 analyzed years. This is likely due to the different geographical distribution of the aviation emissions as explained above.

For the categories anthropogenic non-traffic and shipping, the burden efficiency is roughly the same in both simulations indicating that the larger prescribed NO_x emissions result in a correspondingly large increase of the O_3 production. For the categories biogenic, land transport and biomass burning the burden efficiency is smaller in the simulation EMIS-02 compared to EMIS-01. For the category biogenic, this implies a reduced O_3 production from identical biogenic soil NO_x emissions as the online calculated emissions are identical per set-up definition (see Sect. 2.2.1). For the categories land transport and biomass burning, the NO_x emissions, as well as the O_3 burden, are enhanced in the simulation EMIS-02. However, the emissions and the O_3 burden do not increase uniformly with each other, due to the non-linearity of the O_3 chemistry. For the category lightning on the contrary, the burden efficiency is larger in the simulation EMIS-02 compared to EMIS-01, likely due to the differences in the aviation emissions. The lightning NO_x emissions are identical in the two simulations, but O_3 is produced more efficiently in the simulation EMIS-02.

https://doi.org/10.5194/egusphere-2025-294
Preprint. Discussion started: 24 February 2025

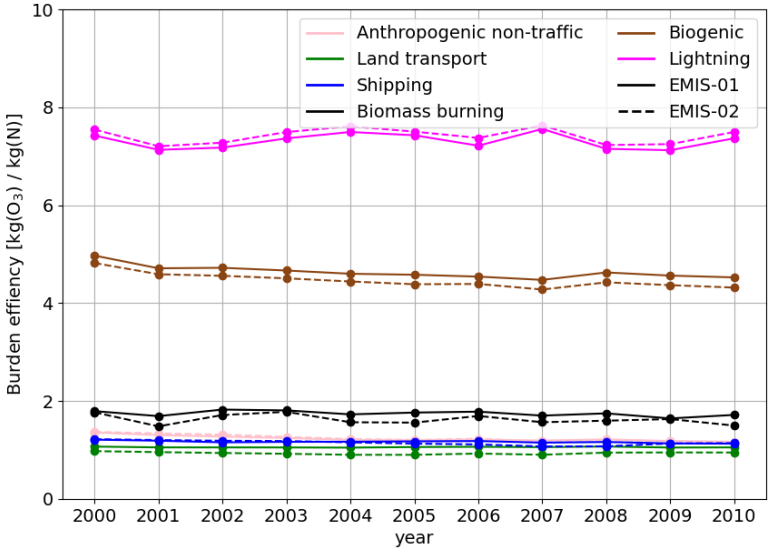

Figure 4. Global burden efficiency χ^i of the categories anthropogenic non-traffic, land transport, shipping, biomass burning, biogenic and lightning (in [kg(O_3) / kg(N)]).

3.2 Contribution to OH and methane lifetime

The results of the analyses of the relative contribution to OH and the associated CH_4 lifetime of the individual categories are presented in this section.

3.2.1 Contribution to OH

Figure 5 shows the zonal mean mixing ratios of OH in both simulations, as well as their difference. The largest differences are located around the tropical tropopause, where the tropospheric OH mixing ratio is largest, and shows larger OH mixing ratios in the simulation EMIS-02 compared to EMIS-01. The OH mixing ratios are also larger in the lower (up to about 500 hPa) tropical troposphere in EMIS-02, but smaller between 500 and 300 hPa.

Figure 6 shows the zonal mean contribution of the categories shipping, anthropogenic non-traffic, land transport, aviation and biomass burning to total OH, as well as the difference of the contribution between the two simulations. A corresponding plot for the categories N_2O decomposition, lightning, stratosphere, CH_4 and biogenic can be found in the supplement (Fig. S5) Zonal means of the year 2000 – 2010 are presented. The OH contributions from the shipping category show maxima in the lower troposphere in the NH in EMIS-01 and in EMIS-02 in the lower troposphere in the NH and SH. The OH contributions from anthropogenic non-traffic and land transport categories show maxima in the lower troposphere in the NH. The aviation category has its maximum in the upper troposphere and above the tropopause in the NH. In the category biomass burning, the

https://doi.org/10.5194/egusphere-2025-294
Preprint. Discussion started: 24 February 2025

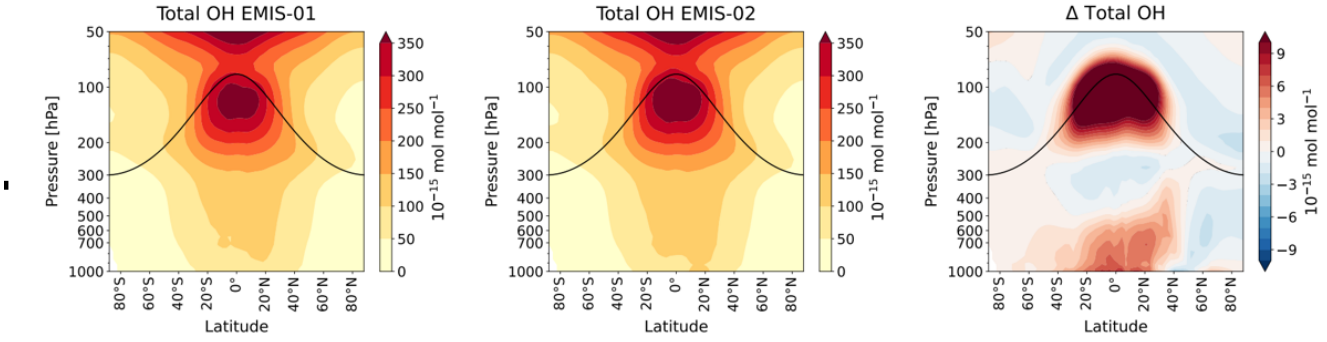

Figure 5. Multi-annual (2000 - 2010), zonally averaged OH volume mixing ratio [10^{-15}mol mol^{-1}] and the absolute differences between EMIS- 01 and EMIS-02 simulation results.

maximum is at the equator in the lower troposphere and in the tropical tropopause region in both simulations. In the simulation EMIS-01, the contribution from the biomass burning category shows another maximum in the northern mid to high latitudes.

The panels in the right column show the differences of the relative contributions of one category to total OH in percentage points between the two simulations. The relative differences indicate that tropospheric OH contributions are not the same for EMIS-01 and EMIS-02. The difference is predominantly positive in all categories, except for the aviation category. In the shipping category, the largest changes in relative OH mixing ratio contribution (10 percentage points) between EMIS-01 and EMIS-02 can be located in the NH and SH up to 900 hPa. The shipping category also shows negative differences (up to -4 percentage points) in a small area in the NH (around 40°N, 1000 hPa). The anthropogenic non-traffic category shows overall positive OH contribution changes with a maximum difference of 4 percentage points around 50°N close to the surface. This category also shows negative differences (up to -3 percentage points) in a small area in the NH (40° – 70°N, 1000 hPa). For the land transport category, the difference (6 percentage points) between the two simulations is most pronounced between 60° and 80°N at 1000 hPa. The land transport category also shows negative differences (- 2 percentage point) in the SH (20° – 80°S, 700 – 1000 hPa). The aviation category indicates a difference of up to 2 percentage points at the tropopause between 70°N and 90°N. This category also shows negative differences (-2 percentage point) between 10°N and 40°N between 250 and 700 hPa. For the biomass burning category, the largest positive differences (4 percentage points) occurs between 0° and 15°S, at 750 – 950 hPa. The biomass burning category also shows negative differences (-7 percentage points) in the NH (around 50° – 70°N, 700 – 900 hPa).

The categories shipping, anthropogenic non-traffic, land transport, aviation and biomass burning show the largest positive and the largest negative differences between EMIS-01 and EMIS-02 with respect to the contribution to OH. The other categories show lower positive and/or lower negative differences (see Fig. S5 in the supplement).

https://doi.org/10.5194/egusphere-2025-294
Preprint. Discussion started: 24 February 2025

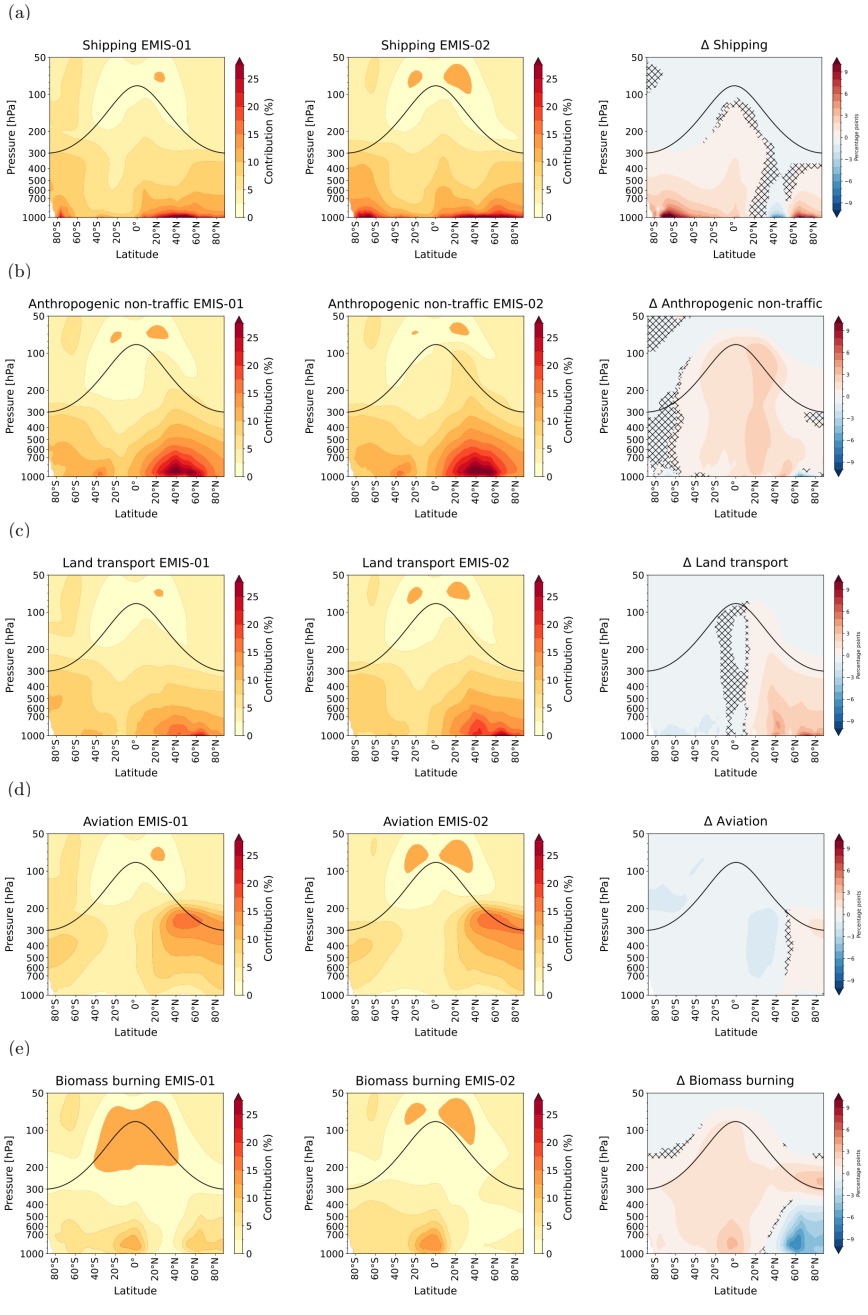

Figure 6. Relative contributions to total OH of the tagging categories (a) shipping, (b) anthropogenic non-traffic, (c) land transport (d) aviation and (e) biomass burning. The left and middle columns show the contribution of the respective category in the simulations EMIS-01 and EMIS-02, respectively. The right column shows the differences of the relative contributions to OH between the two simulation in percentage points. Zonal means of the years 2000 – 2010 are presented. Hatches in the delta plot indicate a p-value ≥ 0.05 from the dependent t-test for paired samples.

https://doi.org/10.5194/egusphere-2025-294
Preprint. Discussion started: 24 February 2025

3.2.2 Contribution to methane lifetime

In this section, we attribute the difference of the tropospheric CH_4 lifetime with respect to the oxidation with OH in the simulations EMIS-01 and EMIS-02 to individual tagging categories. We show results for the NH and SH separately. The black bars in Figure 7 show the total CH_4 lifetime with respect to the oxidation with OH. In the NH, the absolute difference of the total CH_4 lifetime between the simulations EMIS-01 (7.86 years) and EMIS-02 (7.61 years) is -0.25 years, which corresponds to -3.2%. In the SH, the CH_4 lifetime of the simulation EMIS-01 (9.40 years) and EMIS-02 (9.00 years) differs by -0.4 years, which corresponds to -4.3%.

We calculate the contribution of each category to the total CH_4 lifetime change using the two methods, which are explained in Sect. 2.3. The results are shown by the blue and red bars, respectively, in Fig. 7. The relative contributions are consistent for both methods. However, method 1 indicates overall less pronounced CH_4 lifetime changes for the individual categories and underestimates the total CH_4 lifetime change. The sum of all individual contributions calculated using method 2 reproduces the total CH_4 lifetime change well in the NH, and slightly overestimates it in the SH.

Our results show that the anthropogenic non-traffic, land transport, biomass burning, and shipping categories contribute most to the CH_4 reduction from EMIS-01 to EMIS-01 in the NH. In the SH, also the anthropogenic non-traffic, biomass burning and shipping categories contribute to the lifetime reduction. However, the results indicate that the land traffic category leads to a slight extension of CH_4 lifetime in the SH. The impact of the categories N_2O, lightning, stratosphere and CH_4 categories is minor. The aviation category leads to an increase of the CH_4 lifetime in the NH by 0.06 years. The biogenic category leads to an extension of the CH_4 lifetime in both hemispheres.

3.3 Synthesis

We have performed targeted simulations to assess the impact of the changed emission inventories of O_3 precursors (CO, NMHCs, NO_x) from CCMI-1 to CCMI-2022 over the years 2000 - 2010. We find that the changed emission inventories lead to an increase of the tropospheric O_3 column of 3.7%, and to a shortening of the tropospheric CH_4 lifetime by 0.25 years in the NH, which corresponds to 3.2%. In the SH, the tropospheric O_3 column increases by 4.5%, and the tropospheric CH_4 lifetime shortens by 0.4 years, which corresponds to 4.3%. We further use the TAGGING submodel to estimate the contribution of individual tagging categories to the total changes of O_3, OH, and CH_4 lifetime.

In the NH, the largest change of both, the tropospheric O_3 column and the CH_4 lifetime, is attributed to the anthropogenic non-traffic and land transport categories, which correspond to the categories with the largest change of NO_x emissions between CCMI-1 and CCMI-2022 (see Tab. 3). NO_x emissions from the biomass burning are slightly lower by -0.21 Tg(N) in CCMI-2022. This category contributes nevertheless to a shortening of the CH_4 lifetime, which might be explained by the comparable strong reduction (CCMI-2022 compared to CCMI-1) of CO emissions, resulting in an enhanced abundance of OH, as the most important sink of CO is the oxidation with OH (e.g., Nguyen et al., 2020). The tropospheric O_3 column contribution of this category increases slightly. The change of CH_4 lifetime attributed to the shipping category averaged over the analysed 10 years is large compared to the corresponding NO_x emission increase of 0.75 Tg(N) between CCMI-1 and CCMI-2022. The

https://doi.org/10.5194/egusphere-2025-294
Preprint. Discussion started: 24 February 2025

Table 3. Overview of difference of the prescribed emissions, the tropospheric O_3 column, and the tropospheric CH_4 lifetime for the individual tagging categories between the simulations EMIS-02 and EMIS-01. For the contribution of tropospheric CH_4 lifetime change, the estimates derived using method 2 are shown (see Sect. 2.3).

Category	ΔNO_x [Tg(N)]	ΔCO [Tg(C)]	ΔNMHC [Tg(C)]	ΔO_3 [DU]	ΔCH_4 lifetime [years]
Northern Hemisphere					
anthropogenic non-traffic	3.08	7.25	13.70	0.76	-0.15
land transport	2.99	6.68	6.44	0.64	-0.10
biomass burning	-0.21	-36.35	10.00	0.07	-0.08
shipping	0.75	-0.23	0.19	0.16	-0.08
N2O	-	-	-	0.03	0.0
lightning	0.0*	-	-	0.03	0.01
stratosphere	-	-	-	0.07	0.01
CH4	-	-	-	0.00	0.02
aviation	-0.09	0.21	0.07	-0.07	0.06
biogenic	0.0*	0.0	0.0*	-0.27	0.07
residuum	-	-	-	-	-0.01
total	6.51	-22.65	30.40	1.39	-0.25
Southern Hemisphere					
anthropogenic non-traffic	0.34	1.23	8.67	0.51	-0.13
land transport	0.03	1.06	0.91	0.02	0.03
biomass burning	1.62	-8.54	16.88	0.36	-0.19
shipping	0.54	-0.02	0.03	0.37	-0.20
N2O	-	-	-	0.02	0.0
lightning	0.0*	-	-	0.02	-0.02
stratosphere	-	-	-	0.03	0.0
CH4	-	-	-	0.09	0.02
aviation	0.00	0.01	0.005	-0.06	0.04
biogenic	0.0*	0.0	0.0*	-0.18	0.09
residuum	-	-	-	-	-0.05
total	2.19	-7.49	26.50	1.19	-0.4

* Identical online calculated emissions as assured by simulation set-up (see Sect. 2.2.1).

https://doi.org/10.5194/egusphere-2025-294
Preprint. Discussion started: 24 February 2025

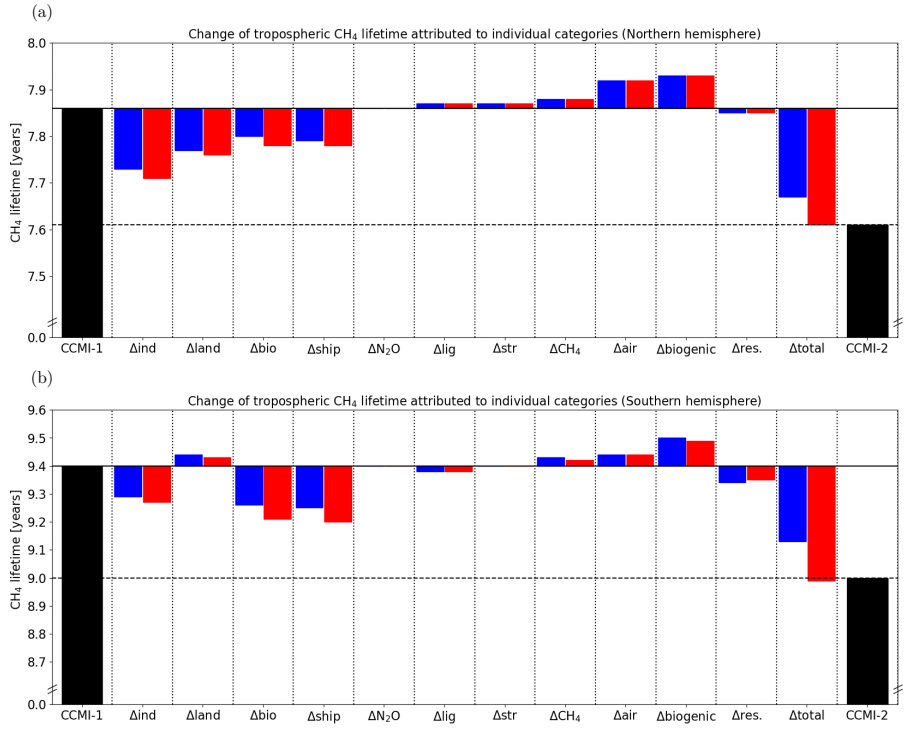

Figure 7. Change of tropospheric CH_4 lifetime attributed to individual tagging categories, separately for the (a) Northern Hemisphere and (b) Southern Hemisphere. The black bars show the CH_4 lifetime with respect to the oxidation with the total OH, $\tau_{CH_4,OH_{total}}$, for the simulations EMIS-01 (CCMI-1) and EMIS-02 (CCMI-2022). The blue and red bars show the contribution of category i to the total CH_4 lifetime change, $\Delta\tau_{CH_4,i}$, calculated either using method 1 (blue) or method 2 (red, see Sect. 2.3 for details on the derivation) . Δtotal is the sum of $\Delta\tau_{CH_4,i}$ over all categories.

difference of NO_x emissions from shipping between CCMI-1 and CCMI-2022 has a distinct temporal evolution peaking in the year 2008 (see Fig. S6), when changes of tropospheric O_3 and CH_4 lifetime of this category are most pronounced. In contrast to the other prescribed emission categories, NO_x from aviation decreases, which is reflected by a decrease of the tropospheric O_3 column and an extension of CH_4 lifetime. In addition, the artificially shifted aviation emissions from the tropics to the polar regions in the CEDS emission inventory, as reported by Thor et al. (2023), can play a role here.

In the SH, the anthropogenic non-traffic, biomass burning, and shipping categories contribute most to the changes of the tropospheric O_3 column and the CH_4 lifetime. In these categories, the increase (CCMI-2022 vs CCMI-1) of NO_x emissions is most pronounced. In addition, CO emissions from biomass burning are also reduced (CCMI-2022 compared to CCMI-1) in the SH. In the SH, the tropospheric O_3 column and the CH_4 lifetime are more sensitive to emission changes, e.g. anthropogenic non-traffic NO_x emission changes are 3.08 Tg(N) in the NH and 0.34 Tg(N) in the SH, which corresponds to increases of the tropospheric O_3 column of 0.76 DU and 0.51 DU, respectively. The land transport and aviation categories play a minor

https://doi.org/10.5194/egusphere-2025-294
Preprint. Discussion started: 24 February 2025

role in the SH. Accordingly, these categories hardly contribute to the tropospheric O_3 column and the CH_4 lifetime difference between the two simulations.

The biogenic category counteracts the increase of the tropospheric O_3 column and the shortening of the CH_4 lifetime in both hemispheres, although biogenic NO_x, CO and NMHC emissions are unchanged (see Tab. 3 and Sect. 2.2.1). The O_3 production efficiency of one category can be affected by emission changes of another category due to non-linear compensation effects (see e.g., Mertens et al., 2018, their Fig. 6). In this case, the diagnosed contribution of the biogenic category to changes of O_3 and CH_4 lifetime is not caused by emission changes, but by a larger O_3 burden efficiency (see Fig. 4).

4 Discussion

4.1 Limitations

First of all, the used TAGGING method relies on some simplifications, which are discussed in more detail by Grewe et al. (2017); Rieger et al. (2018); Mertens et al. (2018). As example, decomposition of PAN from lightning can lead to artificial small contributions of NMHCs from lightning emissions. For the TAGGING of HO_x, a reduced set of chemical reactions is considered, compared to the chemical mechanism calculated by MECCA (Rieger et al., 2018). This means that the sum of all tagged OH tracers can deviate from the total OH tracer. The CH_4 loss unaccounted by the TAGGING, i.e. represented by the residuum lifetime $\tau_{CH_4,res}$ (see Eq. 4), is, however, less important than any of the tagged categories in our simulations. We calculate the contribution of the unaccounted loss to the total CH_4 lifetime change, which is -0.01 years in the NH and -0.05 years in the SH (see Tab. 3). Categories with a smaller contribution are not considered to have a meaningful effect on the CH_4 lifetime change, i.e. N_2O, lightning and stratosphere in the NH, and land transport, N_2O, lightning, stratosphere, CH_4 and aviation in the SH. Further, we calculate the contribution to the CH_4 lifetime change using two methods, which are explained in Sect. 2.3. The relative contributions are consistent for both methods, but only method 2 is closed, meaning that the sum of all individual contributions results in the total change of CH_4 lifetime. Therefore, we recommend to use method 2 for further studies.

Further, our simulation setup does not allow to separate the effects of the individual species, CO, NMHCs, and NO_x. We expect that O_3 production is mainly NO_x limited on the hemispheric scale, and therefore that the changes of NO_x emissions are most important to explain the increase of tropospheric O_3 column and the shortening of the CH_4 lifetime. In general, we find that categories with enhanced NO_x emissions lead to increased tropospheric O_3 column and a shortening of the CH_4 lifetime, which is supporting this assumption. One exception is the biomass burning category in the NH, for which the effect of CO reduction seems to dominate (see Sect. 3.3). For a clear assessment of the effect to the individual species, a different simulation setup, in which only the emissions of either CO, NMHCs, or NO_x are changed, would be necessary.

https://doi.org/10.5194/egusphere-2025-294
Preprint. Discussion started: 24 February 2025

4.2 Comparison to previous results

Previous studies analysing simulation results from other chemistry-climate models prescribing the CEDS emission inventory for O_3 precursor emissions noted a strong shortening of the CH_4 lifetime after the year 1990 as well. For instance, Skeie et al. (2023, their Figure 3) show that the increase of OH is steeper in the AerChemMIP multi-model mean ensemble, which is based on the CEDS emission inventory, compared to the multi-model mean ensemble of CCMI-1. Similarly, the three chemistry-climate models of the AerChemMIP ensemble as analysed by Stevenson et al. (2020) show a drop of the CH_4 lifetime after the year 1990 in the historical simulation, which is not apparent when O_3 precursor emissions are kept at pre-industrial levels. Thus, these studies indicate that the CEDS emission inventory leads to similar effects also in other CCMs, but did not aim at attributing differences to individual emission sectors.

It is noteworthy that both simulations show negative temporal trends of the CH_4 lifetime and positive trends of OH over the period 2000 - 2010, which is in line with the trends simulated by other CCMs (Nicely et al., 2020; Zhao et al., 2020; Stevenson et al., 2020). In line with this, the study by Morgenstern et al. (2025) indicates a positive trend of OH since 1997 based on SH measurements of ^{14}CO. On the contrary, previous observational based estimates and inversions of OH do not indicate a trend (see IPCC, 2021, (Table 6.7) and references therein).

The $CEDS_{GBD\text{-}MAPS}$ emission inventory provided by McDuffie et al. (2020) is an update of CEDS (Hoesly et al., 2018), which suggests smaller global emissions of NO_x and CO after the year 2006 compared to CEDS. The difference is about 3 Tg(N) for NO_x and 10 Tg(C) for CO in the year 2010 (McDuffie et al., 2020, their Figure 6). The differences of NO_x emissions are explained by reduced emissions from the transport sector in India and Africa, and by an updated emission estimate for China (Zheng et al., 2018). The reduction of NO_x emissions in $CEDS_{GBD\text{-}MAPS}$ would compensate about 34% of the NO_x emissions increase from EMIS-01 to EMIS-01, and the increase of CO emissions would compensate about 33% of the reduction of CO emissions from EMIS-01 to EMIS-01. For NMHCs, McDuffie et al. (2020) suggest 5% larger global emissions than Hoesly et al. (2018), which result mainly from larger emissions in Africa from the oil and gas sector.

5 Conclusions

In this study, we analyse the impact of the two different emission inventories for NO_x, CO, and NMHCs, as have been used for the CCMI-1 and CCMI-2022 initiatives, on the simulated tropospheric O_3, OH, and CH_4 lifetime. Therefore, we have performed targeted simulations with the EMAC model over the years 2000 - 2010 equipped with the diagnostic TAGGING submodel to further attribute differences of O_3, OH, and CH_4 lifetime to individual emission sectors (Grewe et al., 2017; Rieger et al., 2018).

Our results suggests that the use of the emission inventory of CCMI-2022 enhances the tropospheric O_3 column by 3.7% in the NH, and by 4.5% in the SH in comparison to the emission inventory used for CCMI-1. The tropospheric CH_4 lifetime with respect to the oxidation with OH shortens by 0.25 years in the NH, and by 0.4 years in the SH.

Using the TAGGING submodel, we attribute these differences to individual emission sectors. In the NH, the sectors contributing most to the change in the tropospheric O_3 column are anthropogenic non-traffic (55%), land transport (46%), shipping

https://doi.org/10.5194/egusphere-2025-294
Preprint. Discussion started: 24 February 2025

(12%), and biomass burning (5%). In the SH, the primary contributors are anthropogenic non-traffic (43%), biomass burning (30%), and shipping (31%). The aviation category counteracts the increase of the tropospheric O_3 column by about 5% in both hemispheres. Due to the non-linearity of the O_3 chemistry, the contributions of tagging categories with unmodified emissions also change. For instance, the O_3 production efficiency of biogenic soil NO_x emissions decreases, which counteracts the increase of the tropospheric O_3 column by 19% in the NH, and by 15% in the SH.

Our study is to our knowledge the first that uses the tagging approach to attribute the difference of CH_4 lifetime between two simulations to individual emission sectors. We find that that the sectors, which contribute most to the increase of the tropospheric O_3 column, also contribute most to the shortening of the tropospheric CH_4 lifetime. However, the contribution of one sector to either the change of O_3 or CH_4 lifetime is not necessarily the same. For instance, in the NH the sector biomass burning contributes about 12% to the increase of the tropospheric O_3 column, but about 32% to the shortening of the CH_4 lifetime.

Further, our results demonstrate the dependence of tropospheric O_3 and the CH_4 lifetime simulated by CCMs on the prescribed emission inventories for NO_x, CO, and NMHCs and the resulting uncertainty. The tropospheric O_3 column and the CH_4 lifetime differ by about 4% for the two used emission inventories that both aim at representing present-day conditions. It would be valuable to investigate whether the change of O_3 and CH_4 lifetime caused by the modified emission inventory are of similar magnitude in other CCMs. The studies by Skeie et al. (2023) and Stevenson et al. (2020) suggest that the CEDS emission inventory leads to a significant shortening of the CH_4 lifetime after the year 1990 in other CCMs as well.

Future research utilizing the tagging method could provide deeper insights into this topic. For example, additional simulations with a revised setup, where only one chemical species (e.g., NO_x) is modified within the emission inventories, would enable a more straightforward comparison of the contributions of NO_x, CO, or NMHC emissions to O_3, OH and the CH_4 lifetime in the troposphere.

Code and data availability. The Modular Earth Submodel System (MESSy; doi: 10.5281/zenodo.8360186) is continuously further developed and applied by a consortium of institutions. The usage of MESSy and access to the source code is licenced to all affiliates of institutions which are members of the MESSy Consortium. Institutions can become a member of the MESSy Consortium by signing the MESSy Memorandum of Understanding. More information can be found on the MESSy Consortium Website (http://www.messy-interface.org). The simulation results presented here are based on MESSy version 2.55.2. The simulation results are archived at zenodo and avaialble under the DOIs 10.5281/zenodo.14712802 (EMIS-01 simulation) and 10.5281/zenodo.14712940 (EMIS-02 simulation).

Appendix A: Derivation of methane lifetime change formula

In this Appendix, we explain how we derived Eq. 5 to calculate $\Delta\tau_{CH_4,i}$, the contribution of category i to the total CH_4 lifetime change. The reciprocal of the total CH_4 lifetime is given by the sum of the reciprocals of the individual lifetimes (see Eq. 3). Here, we use $\tau^{\star}_{CH_4,sum}$, so that the total CH_4 loss by OH including the residuum is accounted for.

https://doi.org/10.5194/egusphere-2025-294
Preprint. Discussion started: 24 February 2025

$$\frac{1}{\tau^{\star}_{CH_4,sum}} = \sum_i \frac{1}{\tau_{CH_4,OH_i}}$$
$$= \frac{1}{\tau_{CH_4,OH_i}} + \sum_{j\neq i} \frac{1}{\tau_{CH_4,OH_j}} \tag{A1}$$

Thus, we can write $\tau^{\star}_{CH_4,sum}$ as a function of τ_{CH_4,OH_i}

$$\tau^{\star}_{CH_4,sum}(\tau_{CH_4,OH_i}) = (\frac{1}{\tau_{CH_4,OH_i}} + \sum_{j\neq i} \frac{1}{\tau_{CH_4,OH_j}})^{-1}, \tag{A2}$$

for which the derivative with respect to τ_{CH_4,OH_i} is given by

$$\frac{d\tau^{\star}_{CH_4,sum}}{d\tau_{CH_4,OH_i}} = (\frac{1}{\tau_{CH_4,OH_i}} + \sum_{j\neq i} \frac{1}{\tau_{CH_4,OH_j}})^{-2} \cdot \tau^{-2}_{CH_4,OH_i}$$
$$= \frac{(\tau^{\star}_{CH_4,sum})^2}{(\tau_{CH_4,OH_i})^2} \tag{A3}$$

Then, we approximate the derivative with the contribution of category i to the total CH_4 lifetime change

$$\frac{\Delta\tau^{\star}_{CH_4,sum}}{\Delta\tau_{CH_4,OH_i}} \simeq \frac{d\tau_{CH_4,sum}}{d\tau_{CH_4,OH_i}}$$
$$\Rightarrow \Delta\tau_{CH_4,i} = \frac{(\tau^{\star}_{CH_4,sum})^2}{(\tau_{CH_4,OH_i})^2} \cdot \Delta\tau_{CH_4,OH_i}. \tag{A4}$$

Author contributions. CA analysed the data, created most of the plots and drafted the manuscript. LS, MM, PJ developed the concept of the study and prepared the simulation setup. All authors contributed to the interpretation of the model results and to writing the manuscript.

Competing interests. At least one author is member of the editorial board of ACP.

Acknowledgements. We thank Alina Fiehn (DLR) for doing the internal review. We used Climate Data Operators (CDO; https://code.mpimet.mpg.de/projects/cdo/, last access: 13 November 2024; Schulzweida, 2023) and netCDF Operators (NCO; Zender, 2024) for data processing. Further, we used Python, especially the packages Xarray (Hoyer and Hamman, 2017) and Matplotlib (Hunter, 2007), for data analysis and producing the figures. We furthermore thank all contributors of the project ESCiMo (Earth System Chemistry integrated Modelling), which provides the model configuration and initial conditions for the model simulations performed here. This work used resources of the Deutsches Klimarechenzentrum (DKRZ) granted by its Scientific Steering Committee (WLA) under project id0853. Further, datasets provided by MESSy via the DKRZ data pool were used.

https://doi.org/10.5194/egusphere-2025-294
Preprint. Discussion started: 24 February 2025

References

Ashmore, M. R.: Assessing the future global impacts of ozone on vegetation, Plant Cell and Environment, 28, 949–964, https://doi.org/10.1111/j.1365-3040.2005.01341.x, 2005.

Bell, M. L., McDermott, A., Zeger, S. L., Samet, J. M., and Dominici, F.: Ozone and short-term mortality in 95 US urban communities, 1987-2000, Jama-Journal of the American Medical Association, 292, 2372–2378, https://doi.org/10.1001/jama.292.19.2372, 2004.

Bourtsoukidis, E., Ernle, L., Crowley, J. N., Lelieveld, J., Paris, J. D., Pozzer, A., Walter, D., and Williams, J.: Non-methane hydrocarbon (C-2-C-8) sources and sinks around the Arabian Peninsula, Atmospheric Chemistry and Physics, 19, 7209–7232, https://doi.org/10.5194/acp-19-7209-2019, 2019.

Brenninkmeijer, C. A. M., Manning, M. R., Lowe, D. C., Wallace, G., Sparks, R. J., and Volz-Thomas, A.: Interhemispheric asymmetry in OH abundance inferred from measurements of atmospheric ^{14}CO, Nature, 356, 50–52, https://doi.org/10.1038/356050a0, 1992.

Butler, T., Lupascu, A., and Nalam, A.: Attribution of ground-level ozone to anthropogenic and natural sources of nitrogen oxides and reactive carbon in a global chemical transport model, Atmospheric Chemistry and Physics, 20, 10 707–10 731, https://doi.org/10.5194/acp-20-10707-2020, 2020.

CCMI-1 simulation protocol: http://www.aparc-climate.org/wp-content/uploads/2017/12/SPARCnewsletter_No40_Jan2013_web.pdf, last accessed: 12-11-2024.

CCMI-2 simulation protocol: https://bpb-eu-w2.wpmucdn.com/blogs.reading.ac.uk/dist/7/201/files/2020/09/CCMI-2022_REF-D1_proposal_20200921.pdf, last accessed: 12-11-2024.

Collins, W. J., Lamarque, J.-F., Schulz, M., Boucher, O., Eyring, V., Hegglin, M. I., Maycock, A., Myhre, G., Prather, M., Shindell, D., and Smith, S. J.: AerChemMIP: quantifying the effects of chemistry and aerosols in CMIP6, Geoscientific Model Development, 10, 585–607, https://doi.org/10.5194/gmd-10-585-2017, 2017.

Crutzen, P. J.: PHOTOCHEMICAL REACTIONS INITIATED BY AND INFLUENCING OZONE IN UNPOLLUTED TROPOSPHERIC AIR, Tellus, 26, 47–57, https://doi.org/10.1111/j.2153-3490.1974.tb01951.x, 1974.

Deckert, R., Jockel, P., Grewe, V., Gottschaldt, K. D., and Hoor, P.: A quasi chemistry-transport model mode for EMAC, Geoscientific Model Development, 4, 195–206, https://doi.org/10.5194/gmd-4-195-2011, 2011.

Emberson, L. D., Pleijel, H., Ainsworth, E. A., van den Berg, M., Ren, W., Osborne, S., Mills, G., Pandey, D., Dentener, F., Buker, P., Ewert, F., Koeble, R., and Van Dingenen, R.: Ozone effects on crops and consideration in crop models, European Journal of Agronomy, 100, 19–34, https://doi.org/10.1016/j.eja.2018.06.002, 2018.

Granier, C., Bessagnet, B., Bond, T., D'Angiola, A., van der Gon, H. D., Frost, G. J., Heil, A., Kaiser, J. W., Kinne, S., Klimont, Z., Kloster, S., Lamarque, J. F., Liousse, C., Masui, T., Meleux, F., Mieville, A., Ohara, T., Raut, J. C., Riahi, K., Schultz, M. G., Smith, S. J., Thompson, A., van Aardenne, J., van der Werf, G. R., and van Vuuren, D. P.: Evolution of anthropogenic and biomass burning emissions of air pollutants at global and regional scales during the 1980-2010 period, Climatic Change, 109, 163–190, https://doi.org/10.1007/s10584-011-0154-1, 2011.

Grewe, V., Brunner, D., Dameris, M., Grenfell, J. L., Hein, R., Shindell, D., and Staehelin, J.: Origin and variability of upper tropospheric nitrogen oxides and ozone at northern mid-latitudes, Atmospheric Environment, 35, 3421–3433, https://doi.org/10.1016/s1352-2310(01)00134-0, 2001.

Grewe, V., Tsati, E., and Hoor, P.: On the attribution of contributions of atmospheric trace gases to emissions in atmospheric model applications, Geoscientific Model Development, 3, 487–499, https://doi.org/10.5194/gmd-3-487-2010, 2010.

https://doi.org/10.5194/egusphere-2025-294
Preprint. Discussion started: 24 February 2025

Grewe, V., Dahlmann, K., Matthes, S., and Steinbrecht, W.: Attributing ozone to NOx emissions: Implications for climate mitigation measures, Atmospheric Environment, 59, 102–107, https://doi.org/10.1016/j.atmosenv.2012.05.002, 2012.

Grewe, V., Tsati, E., Mertens, M., Fromming, C., and Jockel, P.: Contribution of emissions to concentrations: the TAGGING 1.0 submodel based on the Modular Earth Submodel System (MESSy 2.52), Geoscientific Model Development, 10, 2615–2633, https://doi.org/10.5194/gmd-10-2615-2017, 2017.

Guenther, A., Hewitt, C. N., Erickson, D., Fall, R., Geron, C., Graedel, T., Harley, P., Klinger, L., Lerdau, M., McKay, W. A., Pierce, T., Scholes, B., Steinbrecher, R., Tallamraju, R., Taylor, J., and Zimmerman, P.: A GLOBAL-MODEL OF NATURAL VOLATILE ORGANIC-COMPOUND EMISSIONS, Journal of Geophysical Research-Atmospheres, 100, 8873–8892, https://doi.org/10.1029/94jd02950, 1995.

Haagensmit, A. J.: CHEMISTRY AND PHYSIOLOGY OF LOS-ANGELES SMOG, Industrial and Engineering Chemistry, 44, 1342–1346, https://doi.org/10.1021/ie50510a045, 1952.

Hersbach, H., Bell, B., Berrisford, P., Hirahara, S., Horanyi, A., Munoz-Sabater, J., Nicolas, J., Peubey, C., Radu, R., Schepers, D., Simmons, A., Soci, C., Abdalla, S., Abellan, X., Balsamo, G., Bechtold, P., Biavati, G., Bidlot, J., Bonavita, M., De Chiara, G., Dahlgren, P., Dee, D., Diamantakis, M., Dragani, R., Flemming, J., Forbes, R., Fuentes, M., Geer, A., Haimberger, L., Healy, S., Hogan, R. J., Holm, E., Janiskova, M., Keeley, S., Laloyaux, P., Lopez, P., Lupu, C., Radnoti, G., de Rosnay, P., Rozum, I., Vamborg, F., Villaume, S., and Thepaut, J. N.: The ERA5 global reanalysis, Quarterly Journal of the Royal Meteorological Society, 146, 1999–2049, https://doi.org/10.1002/qj.3803, 2020.

Hoesly, R. M., Smith, S. J., Feng, L. Y., Klimont, Z., Janssens-Maenhout, G., Pitkanen, T., Seibert, J. J., Vu, L., Andres, R. J., Bolt, R. M., Bond, T. C., Dawidowski, L., Kholod, N., Kurokawa, J., Li, M., Liu, L., Lu, Z. F., Moura, M. C. P., O'Rourke, P. R., and Zhang, Q.: Historical (1750-2014) anthropogenic emissions of reactive gases and aerosols from the Community Emissions Data System (CEDS), Geoscientific Model Development, 11, 369–408, https://doi.org/10.5194/gmd-11-369-2018, 2018.

Hoyer, S. and Hamman, J.: xarray: N-D labeled arrays and datasets in Python, Journal of Open Research Software, 5, https://doi.org/10.5334/jors.148, 2017.

Hunter, J. D.: Matplotlib: A 2D graphics environment, Comput Sci Eng, 9, 90–95, https://doi.org/10.1109/MCSE.2007.55, 2007.

Iglesias, D. J., Calatayud, A., Barreno, E., Primo-Millo, E., and Talon, M.: Responses of citrus plants to ozone: leaf biochemistry, antioxidant mechanisms and lipid peroxidation, Plant Physiology and Biochemistry, 44, 125–131, https://doi.org/10.1016/j.plaphy.2006.03.007, 2006.

IPCC: Climate Change 2013: The Physical Science Basis. Contribution of Working Group I to the Fifth Assessment Report of the Intergovernmental Panel on Climate Change [Stocker, T.F., D. Qin, G.-K. Plattner, M. Tignor, S.K. Allen, J. Boschung, A. Nauels, Y. Xia, V. Bex and P.M. Midgley (eds.)]. Cambridge University Press, Cambridge, United Kingdom and New York, NY, USA, 1535 pp., 2013.

IPCC: Climate Change 2021: The Physical Science Basis. Contribution of Working Group I to the Sixth Assessment Report of the Intergovernmental Panel on Climate Change. Masson-Delmotte, V., P. Zhai, A. Pirani, S.L. Connors, C. Péan, S. Berger, N. Caud, Y. Chen, L. Goldfarb, M.I. Gomis, M. Huang, K. Leitzell, E. Lonnoy, J.B.R. Matthews, T.K. Maycock, T. Waterfield, O. Yelekçi, R. Yu, and B. Zhou (eds.). Cambridge University Press, Cambridge, United Kingdom and New York, NY, USA, 2391 pp., 2021.

Jerrett, M., Burnett, R. T., Pope, C. A., Ito, K., Thurston, G., Krewski, D., Shi, Y. L., Calle, E., and Thun, M.: Long-Term Ozone Exposure and Mortality, New England Journal of Medicine, 360, 1085–1095, https://doi.org/10.1056/NEJMoa0803894, 2009.

Jöckel, P.: CCMI-2022: refD1 data produced by the EMAC-CCMI2 model at MESSy-Consortium, https://catalogue.ceda.ac.uk/uuid/9b15ae551fda4035a7940a3adbe31691/, 2023.

Jöckel, P., Brenninkmeijer, C. A. M., Lawrence, M. G., Jeuken, A. B. M., and van Velthoven, P. F. J.: Evaluation of stratosphere–troposphere exchange and the hydroxyl radical distribution in three-dimensional global atmospheric models using observations of cosmogenic ^{14}CO,

https://doi.org/10.5194/egusphere-2025-294
Preprint. Discussion started: 24 February 2025

Journal of Geophysical Research: Atmospheres, 107, ACH 12–1–ACH 12–18, https://doi.org/https://doi.org/10.1029/2001JD001324, 2002.

Jöckel, P., Sander, R., Kerkweg, A., Tost, H., and Lelieveld, J.: Technical note: The Modular Earth Submodel System (MESSy) - a new approach towards Earth System Modeling, Atmospheric Chemistry and Physics, 5, 433–444, <GotoISI>://WOS:000226908300005, 2005.

Jöckel, P., Kerkweg, A., Pozzer, A., Sander, R., Tost, H., Riede, H., Baumgaertner, A., Gromov, S., and Kern, B.: Development cycle 2 of the Modular Earth Submodel System (MESSy2), Geoscientific Model Development, 3, 717–752, https://doi.org/10.5194/gmd-3-717-2010, 2010.

Jöckel, P., Tost, H., Pozzer, A., Kunze, M., Kirner, O., Brenninkmeijer, C. A. M., Brinkop, S., Cai, D. S., Dyroff, C., Eckstein, J., Frank, F., Garny, H., Gottschaldt, K. D., Graf, P., Grewe, V., Kerkweg, A., Kern, B., Matthes, S., Mertens, M., Meul, S., Neumaier, M., Nutzel, M., Oberlander-Hayn, S., Ruhnke, R., Runde, T., Sander, R., Scharffe, D., and Zahn, A.: Earth System Chemistry integrated Modelling (ESCiMo) with the Modular Earth Submodel System (MESSy) version 2.51, Geoscientific Model Development, 9, 1153–1200, https://doi.org/10.5194/gmd-9-1153-2016, 2016.

Kerkweg, A., Sander, R., Tost, H., and Jockel, P.: Technical note: Implementation of prescribed (OFFLEM), calculated (ONLEM), and pseudo-emissions (TNUDGE) of chemical species in the Modular Earth Submodel System (MESSy), Atmospheric Chemistry and Physics, 6, 3603–3609, https://doi.org/10.5194/acp-6-3603-2006, 2006.

Kilian, M., Grewe, V., Jöckel, P., Kerkweg, A., Mertens, M., Zahn, A., and Ziereis, H.: Ozone source attribution in polluted European areas during summer 2017 as simulated with MECO(n), Atmospheric Chemistry and Physics, 24, 13 503–13 523, https://doi.org/10.5194/acp-24-13503-2024, 2024.

Krol, M., van Leeuwen, P. J., and Lelieveld, J.: Global OH trend inferred from methylchloroform measurements, Journal of Geophysical Research: Atmospheres, 103, 10 697–10 711, https://doi.org/https://doi.org/10.1029/98JD00459, 1998.

Lamarque, J. F., Hess, P., Emmons, L., Buja, L., Washington, W., and Granier, C.: Tropospheric ozone evolution between 1890 and 1990, Journal of Geophysical Research-Atmospheres, 110, https://doi.org/10.1029/2004jd005537, 2005.

Lawrence, M. G., Jöckel, and von Kuhlmann, R.: What does the global mean OH concentration tell us?, Atmos. Chem. Phys., 1, 37–49, https://doi.org/10.5194/acp-1-37-2001, 2001.

Lelieveld, J., Gromov, S., Pozzer, A., and Taraborrelli, D.: Global tropospheric hydroxyl distribution, budget and reactivity, Atmospheric Chemistry and Physics, 16, 12 477–12 493, https://doi.org/10.5194/acp-16-12477-2016, 2016.

Manning, M. R., Lowe, D. C., Moss, R. C., Bodeker, G. E., and Allan, W.: Short-term variations in the oxidizing power of the atmosphere, Nature, 436, 1001–1004, https://doi.org/10.1038/nature03900, 2005.

McDuffie, E. E., Smith, S. J., O'Rourke, P., Tibrewal, K., Venkataraman, C., Marais, E. A., Zheng, B., Crippa, M., Brauer, M., and Martin, R. V.: A global anthropogenic emission inventory of atmospheric pollutants from sector- and fuel-specific sources (1970–2017): an application of the Community Emissions Data System (CEDS), Earth System Science Data, 12, 3413–3442, https://doi.org/10.5194/essd-12-3413-2020, 2020.

Mertens, M., Grewe, V., Rieger, V. S., and Jockel, P.: Revisiting the contribution of land transport and shipping emissions to tropospheric ozone, Atmospheric Chemistry and Physics, 18, 5567–5588, https://doi.org/10.5194/acp-18-5567-2018, 2018.

Mertens, M., Kerkweg, A., Volker, G., Jockel, P., and Sausen, R.: Attributing ozone and its precursors to land transport emissions in Europe and Germany, Atmospheric Chemistry and Physics, 20, 7843–7873, https://doi.org/10.5194/acp-20-7843-2020, 2020.

https://doi.org/10.5194/egusphere-2025-294
Preprint. Discussion started: 24 February 2025

Mertens, M., Brinkop, S., Graf, P., Grewe, V., Hendricks, J., Jöckel, P., Lanteri, A., Matthes, S., Rieger, V. S., Righi, M., and Thor, R. N.: The contribution of transport emissions to ozone mixing ratios and methane lifetime in 2015 and 2050 in the Shared Socioeconomic Pathways (SSPs), Atmospheric Chemistry and Physics, 24, 12 079–12 106, https://doi.org/10.5194/acp-24-12079-2024, 2024.

Monks, P. S.: Gas-phase radical chemistry in the troposphere, Chemical Society Reviews, 34, 376–395, https://doi.org/10.1039/b307982c, 2005.

Monks, P. S., Archibald, A. T., Colette, A., Cooper, O., Coyle, M., Derwent, R., Fowler, D., Granier, C., Law, K. S., Mills, G. E., Stevenson, D. S., Tarasova, O., Thouret, V., von Schneidemesser, E., Sommariva, R., Wild, O., and Williams, M. L.: Tropospheric ozone and its precursors from the urban to the global scale from air quality to short-lived climate forcer, Atmospheric Chemistry and Physics, 15, 8889–8973, https://doi.org/10.5194/acp-15-8889-2015, 2015.

Montzka, S. A., Krol, M., Dlugokencky, E., Hall, B., Jöckel, P., and Lelieveld, J.: Small Interannual Variability of Global Atmospheric Hydroxyl, Science, 331, 67–69, https://doi.org/10.1126/science.1197640, 2011.

Morgenstern, O., Moss, R., Manning, M., Zeng, G., Schaefer, H., Usoskin, I., Turnbull, J., Brailsford, G., Nichol, S., and Bromley, T.: Radiocarbon monoxide indicates increasing atmospheric oxidizing capacity, Nature Communications, 16, https://doi.org/10.1038/s41467-024-55603-1, 2025.

Moura, B. B., Alves, E. S., de Souza, S. R., Domingos, M., and Vollenweider, P.: Ozone phytotoxic potential with regard to fragments of the Atlantic Semi-deciduous Forest downwind of Sao Paulo, Brazil, Environmental Pollution, 192, 65–73, https://doi.org/10.1016/j.envpol.2014.05.014, 2014.

Myhre, G., Shindell, D., Bréon, F.-M., Collins, W., Fuglestvedt, J., Huang, J., Koch, D., Lamarque, J.-F., Lee, D., Mendoza, B., Nakajima, T., Robock, A., Stephens, G., Takemura, T., and Zhang, H.: Anthropogenic and Natural Radiative Forcing. Climate Change 2013: The Physical Science Basis. Contribution of Working Group I to the Fifth Assessment Report of the Intergovernmental Panel on Climate Change [Stocker, T.F., D. Qin, G.-K. Plattner, M. Tignor, S.K. Allen, J. Boschung, A. Nauels, Y. Xia, V. Bex and P.M. Midgley (eds.)], Cambridge University Press, Cambridge, United Kingdom and New York, NY, USA, https://doi.org/10.1017/CBO9781107415324.018, 2013.

Nguyen, N. H., Turner, A. J., Yin, Y., Prather, M. J., and Frankenberg, C.: Effects of Chemical Feedbacks on Decadal Methane Emissions Estimates, Geophysical Research Letters, 47, e2019GL085 706, https://doi.org/https://doi.org/10.1029/2019GL085706, e2019GL085706 10.1029/2019GL085706, 2020.

Nicely, J. M., Duncan, B. N., Hanisco, T. F., Wolfe, G. M., Salawitch, R. J., Deushi, M., Haslerud, A. S., Jöckel, P., Josse, B., Kinnison, D. E., Klekociuk, A., Manyin, M. E., Marécal, V., Morgenstern, O., Murray, L. T., Myhre, G., Oman, L. D., Pitari, G., Pozzer, A., Quaglia, I., Revell, L. E., Rozanov, E., Stenke, A., Stone, K., Strahan, S., Tilmes, S., Tost, H., Westervelt, D. M., and Zeng, G.: A machine learning examination of hydroxyl radical differences among model simulations for CCMI-1, Atmospheric Chemistry and Physics, 20, 1341–1361, https://doi.org/10.5194/acp-20-1341-2020, 2020.

Niemeier, U., Granier, C., Kornblueh, L., Walters, S., and Brasseur, G. P.: Global impact of road traffic on atmospheric chemical composition and on ozone climate forcing, Journal of Geophysical Research-Atmospheres, 111, https://doi.org/10.1029/2005jd006407, 2006.

Nuvolone, D., Petri, D., and Voller, F.: The effects of ozone on human health, Environmental Science and Pollution Research, 25, 8074–8088, https://doi.org/10.1007/s11356-017-9239-3, 2018.

Prather, M. J., Holmes, C. D., and Hsu, J.: Reactive greenhouse gas scenarios: Systematic exploration of uncertainties and the role of atmospheric chemistry, Geophys. Res. Lett., 39, https://doi.org/10.1029/2012GL051440, 2012.

https://doi.org/10.5194/egusphere-2025-294
Preprint. Discussion started: 24 February 2025

Prinn, R. G., Huang, J., Weiss, R. F., Cunnold, D. M., Fraser, P. J., Simmonds, P. G., McCulloch, A., Harth, C., Reimann, S., Salameh, P., O'Doherty, S., Wang, R. H. J., Porter, L. W., Miller, B. R., and Krummel, P. B.: Evidence for variability of atmospheric hydroxyl radicals over the past quarter century, Geophys. Res. Lett., 32, https://doi.org/10.1029/2004GL022228, 2005.

Rieger, V. S., Mertens, M., and Grewe, V.: An advanced method of contributing emissions to short-lived chemical species (OH and HO2): the TAGGING 1.1 submodel based on the Modular Earth Submodel System (MESSy 2.53), Geoscientific Model Development, 11, 2049–2066, https://doi.org/10.5194/gmd-11-2049-2018, 2018.

Roeckner, E., Brokopf, R., Esch, M., Giorgetta, M., Hagemann, S., Kornblueh, L., Manzini, E., Schlese, U., and Schulzweida, U.: Sensitivity of Simulated Climate to Horizontal and Vertical Resolution in the ECHAM5 Atmosphere Model, Journal of Climate, 19, 3771 – 3791, https://doi.org/10.1175/JCLI3824.1, 2006.

Sander, R., Baumgaertner, A., Cabrera-Perez, D., Frank, F., Gromov, S., Grooß, J.-U., Harder, H., Huijnen, V., Jöckel, P., Karydis, V. A., Niemeyer, K. E., Pozzer, A., Riede, H., Schultz, M. G., Taraborrelli, D., and Tauer, S.: The community atmospheric chemistry box model CAABA/MECCA-4.0, Geoscientific Model Development, 12, 1365–1385, https://doi.org/10.5194/gmd-12-1365-2019, 2019.

Saunois, M., Stavert, A. R., Poulter, B., Bousquet, P., Canadell, J. G., Jackson, R. B., Raymond, P. A., Dlugokencky, E. J., Houweling, S., Patra, P. K., Ciais, P., Arora, V. K., Bastviken, D., Bergamaschi, P., Blake, D. R., Brailsford, G., Bruhwiler, L., Carlson, K. M., Carrol, M., Castaldi, S., Chandra, N., Crevoisier, C., Crill, P. M., Covey, K., Curry, C. L., Etiope, G., Frankenberg, C., Gedney, N., Hegglin, M. I., Höglund-Isaksson, L., Hugelius, G., Ishizawa, M., Ito, A., Janssens-Maenhout, G., Jensen, K. M., Joos, F., Kleinen, T., Krummel, P. B., Langenfelds, R. L., Laruelle, G. G., Liu, L., Machida, T., Maksyutov, S., McDonald, K. C., McNorton, J., Miller, P. A., Melton, J. R., Morino, I., Müller, J., Murguia-Flores, F., Naik, V., Niwa, Y., Noce, S., O'Doherty, S., Parker, R. J., Peng, C., Peng, S., Peters, G. P., Prigent, C., Prinn, R., Ramonet, M., Regnier, P., Riley, W. J., Rosentreter, J. A., Segers, A., Simpson, I. J., Shi, H., Smith, S. J., Steele, L. P., Thornton, B. F., Tian, H., Tohjima, Y., Tubiello, F. N., Tsuruta, A., Viovy, N., Voulgarakis, A., Weber, T. S., van Weele, M., van der Werf, G. R., Weiss, R. F., Worthy, D., Wunch, D., Yin, Y., Yoshida, Y., Zhang, W., Zhang, Z., Zhao, Y., Zheng, B., Zhu, Q., Zhu, Q., and Zhuang, Q.: The Global Methane Budget 2000–2017, Earth Syst. Sci. Data, 12, 1561–1623, https://doi.org/10.5194/essd-12-1561-2020, 2020.

Schultz, M., Rast, S., van het Bolscher, M., Pulles, T., Pereira, J.and Spessa, A., Dalsøren, S.and van Nojie, T., and Szopa, S.: REanalysis of the TROpospheric chemical composition over the past 40 years, A long-term global modeling study of tropospheric chemistry funded under the 5th EU framework programme. Tech. rep., EU-Contract No., 2007.

Schulzweida, U.: CDO User Guide (2.3.0), Zenodo, https://doi.org/10.5281/zenodo.10020800, 2023.

Schumann, U. and Huntrieser, H.: The global lightning-induced nitrogen oxides source, Atmospheric Chemistry and Physics, 7, 3823–3907, https://doi.org/10.5194/acp-7-3823-2007, 2007.

Seinfeld, J. H. and Pandis, S. N.: Atmospheric chemistry and physics: from air pollution to climate change, John Wiley & Sons, Inc., 3rd edn., 2016.

Silva, R. A., West, J. J., Zhang, Y. Q., Anenberg, S. C., Lamarque, J. F., Shindell, D. T., Collins, W. J., Dalsoren, S., Faluvegi, G., Folberth, G., Horowitz, L. W., Nagashima, T., Naik, V., Rumbold, S., Skeie, R., Sudo, K., Takemura, T., Bergmann, D., Cameron-Smith, P., Cionni, I., Doherty, R. M., Eyring, V., Josse, B., MacKenzie, I. A., Plummer, D., Righi, M., Stevenson, D. S., Strode, S., Szopa, S., and Zeng, G.: Global premature mortality due to anthropogenic outdoor air pollution and the contribution of past climate change, Environmental Research Letters, 8, https://doi.org/10.1088/1748-9326/8/3/034005, 2013.

Skeie, R. B., Hodnebrog, Ø., and Myhre, G.: Trends in atmospheric methane concentrations since 1990 were driven and modified by anthropogenic emissions, Commun Earth Environ, 4, 317, https://doi.org/10.1038/s43247-023-00969-1, 2023.

https://doi.org/10.5194/egusphere-2025-294
Preprint. Discussion started: 24 February 2025

Stecher, L. M.: The role of methane for chemistry-climate interactions, http://nbn-resolving.de/urn:nbn:de:bvb:19-338123, 2024.

Stevenson, D. S., Young, P. J., Naik, V., Lamarque, J. F., Shindell, D. T., Voulgarakis, A., Skeie, R. B., Dalsoren, S. B., Myhre, G., Berntsen, T. K., Folberth, G. A., Rumbold, S. T., Collins, W. J., MacKenzie, I. A., Doherty, R. M., Zeng, G., van Noije, T. P. C., Strunk, A., Bergmann, D., Cameron-Smith, P., Plummer, D. A., Strode, S. A., Horowitz, L., Lee, Y. H., Szopa, S., Sudo, K., Nagashima, T., Josse, B., Cionni, I., Righi, M., Eyring, V., Conley, A., Bowman, K. W., Wild, O., and Archibald, A.: Tropospheric ozone changes, radiative forcing and attribution to emissions in the Atmospheric Chemistry and Climate Model Intercomparison Project (ACCMIP), Atmospheric Chemistry and Physics, 13, 3063–3085, https://doi.org/10.5194/acp-13-3063-2013, 2013.

Stevenson, D. S., Zhao, A., Naik, V., O'Connor, F. M., Tilmes, S., Zeng, G., Murray, L. T., Collins, W. J., Griffiths, P. T., Shim, S. B., Horowitz, L. W., Sentman, L. T., and Emmons, L.: Trends in global tropospheric hydroxyl radical and methane lifetime since 1850 from AerChemMIP, Atmospheric Chemistry and Physics, 20, 12 905–12 920, https://doi.org/10.5194/acp-20-12905-2020, 2020.

Szopa, S., Naik, V., Adhikary, B., Artaxo, P., Berntsen, T., Collins, W., Fuzzi, S., Gallardo, L., Kiendler-Scharr, A., Klimont, Z., H. Liao, N. U., , and Zanis, P.: Short-Lived Climate Forcers. Climate Change 2021: The Physical Science Basis. Contribution of Working Group I to the Sixth Assessment Report of the Intergovernmental Panel on Climate Change [Masson-Delmotte, V., P. Zhai, A. Pirani, S.L. Connors, C. Péan, S. Berger, N. Caud, Y. Chen, L. Goldfarb, M.I. Gomis, M. Huang, K. Leitzell, E. Lonnoy, J.B.R. Matthews, T.K. Maycock, T. Waterfield, O. Yelekçi, R. Yu, and B. Zhou (eds.)], pp. 817—-922, Cambridge University Press, Cambridge, United Kingdom and New York, NY, USA, https://doi.org/10.1017/9781009157896.008, 2021.

Thor, R. N., Mertens, M., Matthes, S., Righi, M., Hendricks, J., Brinkop, S., Graf, P., Grewe, V., Jöckel, P., and Smith, S.: An inconsistency in aviation emissions between CMIP5 and CMIP6 and the implications for short-lived species and their radiative forcing, Geoscientific Model Development, 16, 1459–1466, https://doi.org/10.5194/gmd-16-1459-2023, 2023.

Uherek, E., Halenka, T., Borken-Kleefeld, J., Balkanski, Y., Berntsen, T., Borrego, C., Gauss, M., Hoor, P., Juda-Rezler, K., Lelieveld, J., Melas, D., Rypdal, K., and Schmid, S.: Transport impacts on atmosphere and climate: Land transport, Atmospheric Environment, 44, 4772–4816, https://doi.org/10.1016/j.atmosenv.2010.01.002, 2010.

van der Werf, G. R., Randerson, J. T., Giglio, L., Collatz, G. J., Kasibhatla, P. S., and Arellano, A. F.: Interannual variability in global biomass burning emissions from 1997 to 2004, Atmospheric Chemistry and Physics, 6, 3423–3441, https://doi.org/10.5194/acp-6-3423-2006, 2006.

van Marle, M. J. E., Kloster, S., Magi, B. I., Marlon, J. R., Daniau, A.-L., Field, R. D., Arneth, A., Forrest, M., Hantson, S., Kehrwald, N. M., Knorr, W., Lasslop, G., Li, F., Mangeon, S., Yue, C., Kaiser, J. W., and van der Werf, G. R.: Historic global biomass burning emissions for CMIP6 (BB4CMIP) based on merging satellite observations with proxies and fire models (1750–2015), Geoscientific Model Development, 10, 3329–3357, https://doi.org/10.5194/gmd-10-3329-2017, 2017.

Vinken, G. C. M., Boersma, K. F., Maasakkers, J. D., Adon, M., and Martin, R. V.: Worldwide biogenic soil NOx emissions inferred from OMI NO2 observations, Atmospheric Chemistry and Physics, 14, 10 363–10 381, https://doi.org/10.5194/acp-14-10363-2014, 2014.

Voulgarakis, A., Naik, V., Lamarque, J. F., Shindell, D. T., Young, P. J., Prather, M. J., Wild, O., Field, R. D., Bergmann, D., Cameron-Smith, P., Cionni, I., Collins, W. J., Dalsoren, S. B., Doherty, R. M., Eyring, V., Faluvegi, G., Folberth, G. A., Horowitz, L. W., Josse, B., MacKenzie, I. A., Nagashima, T., Plummer, D. A., Righi, M., Rumbold, S. T., Stevenson, D. S., Strode, S. A., Sudo, K., Szopa, S., and Zeng, G.: Analysis of present day and future OH and methane lifetime in the ACCMIP simulations, Atmospheric Chemistry and Physics, 13, 2563–2587, https://doi.org/10.5194/acp-13-2563-2013, 2013.

Wedow, J. M., Ainsworth, E. A., and Li, S.: Plant biochemistry influences tropospheric ozone formation, destruction, deposition, and response, Trends in Biochemical Sciences, 46, 992–1002, https://doi.org/10.1016/j.tibs.2021.06.007, 2021.

https://doi.org/10.5194/egusphere-2025-294
Preprint. Discussion started: 24 February 2025

Yienger, J. J. and Levy II, H.: Empirical model of global soil-biogenic NO_x emissions, Journal of Geophysical Research: Atmospheres, 100, 11 447–11 464, https://doi.org/https://doi.org/10.1029/95JD00370, 1995.

Young, P. J., Archibald, A. T., Bowman, K. W., Lamarque, J. F., Naik, V., Stevenson, D. S., Tilmes, S., Voulgarakis, A., Wild, O., Bergmann, D., Cameron-Smith, P., Cionni, I., Collins, W. J., Dalsoren, S. B., Doherty, R. M., Eyring, V., Faluvegi, G., Horowitz, L. W., Josse, B., Lee, Y. H., MacKenzie, I. A., Nagashima, T., Plummer, D. A., Righi, M., Rumbold, S. T., Skeie, R. B., Shindell, D. T., Strode, S. A., Sudo, K., Szopa, S., and Zeng, G.: Pre-industrial to end 21st century projections of tropospheric ozone from the Atmospheric Chemistry and Climate Model Intercomparison Project (ACCMIP), Atmospheric Chemistry and Physics, 13, 2063–2090, https://doi.org/10.5194/acp-13-2063-2013, 2013.

Zender, C. S.: netCDF Operator (NCO) User Guide, http://nco.sf.net/nco.pdf, 2024.

Zhao, Y., Saunois, M., Bousquet, P., Lin, X., Berchet, A., Hegglin, M. I., Canadell, J. G., Jackson, R. B., Deushi, M., Jöckel, P., Kinnison, D., Kirner, O., Strode, S., Tilmes, S., Dlugokencky, E. J., and Zheng, B.: On the role of trend and variability in the hydroxyl radical (OH) in the global methane budget, Atmospheric Chemistry and Physics, 20, 13 011–13 022, https://doi.org/10.5194/acp-20-13011-2020, 2020.

Zheng, B., Tong, D., Li, M., Liu, F., Hong, C., Geng, G., Li, H., Li, X., Peng, L., Qi, J., Yan, L., Zhang, Y., Zhao, H., Zheng, Y., He, K., and Zhang, Q.: Trends in China's anthropogenic emissions since 2010 as the consequence of clean air actions, Atmos. Chem. Phys., 18, 14 095–14 111, https://doi.org/10.5194/acp-18-14095-2018, 2018.